PERFORMANCE EVALUATION OF POLYURETHANE COMPOSITES USING

VACUUM INFUSION PROCESS


by


MOHANED M. MOHAMED


A DISSERTATION

Presented to the Faculty of the Graduate School of the

MISSOURI UNIVERSITY OF SCIENCE AND TECHNOLOGY

In Partial Fulfillment of the Requirements for the Degree


DOCTOR OF PHILOSOPHY

in

MECHANICAL ENGINEERING


2014


Approved
K. Chandrashekhara, Advisor
L. R. Dharani
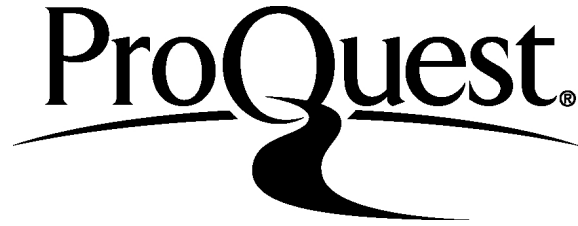Cheng Wang
Vy Khoi Le
X. Du

ProQuest Number: 10133197

ProQuest 10133197

## PUBLICATION DISSERTATION OPTION

This dissertation has been prepared in the form of three papers for publication. Pages 7-36 have been published in Advanced Composite Materials journal. Pages 37-65 have been accepted for publication in Polymers and Polymer Composites journal. Pages 66-97 are intended for submission to Composite Structures journal.

**ABSTRACT**

Glass fiber-reinforced polymer composites have promising applications in infrastructures due to their low cost, high specific stiffness/strength, and corrosion resistance. The pultrusion process is often used to manufacture glass fiber-reinforced polyurethane (PU) composite. The objective of this study is to use thermoset PU resin to manufacture high quality composites for infrastructure applications using vacuum assisted resin transfer molding (VARTM) process. Using VARTM to fabricate PU resins presents unique challenges. Several modifications however have helped with overcoming these problems. In part I of the research, the mechanical performance of two different PU resin not only evaluated but also compared to one another. These results were used to determine which PU should be used in the next two parts. The composite panels were fabricated using VARTM process. In part II. VARTM process was used to fabricate reinforced PU composite bridge deck. The bending stiffness, load carrying capacity, and compressive properties of composite bridge deck panels were each evaluated. Commercial finite element software ABAQUS was used to analyze the panels under bending. In part III, design and manufacture composite structure insulation panels were investigated. Development of composites housing requires a unique design approach with components performing several functions beyond carrying mechanical. To meet these challenges, innovative processing techniques combined with new materials technology developed and evaluated. VARTM manufacturing process modified to manufacture multifunctional panels for housing and army shelter applications. A series of mechanical tests were performed on these structural components.

**DEDICATION**

I would like to dedicate this work to my parents for their continued support.

Without their encouragements, I would not be able to accomplish and fulfill my dreams.

Unfortunately, both of them have passed away during my study at Missouri S&T.

I owe a debt of gratitude to my parents which I can never repay.

# ACKNOWLEDGMENTS

I would like to express my deepest gratitude to my advisor, Dr. K Chandrashekhara, for his excellent guidance, care, patience. Dr. Chandrashekhara provided me with an excellent learning environment at Missouri University of Science and Technology. It has been a great pleasure to work with him.

I want to extend my genuine appreciation to my advisory committee members, Dr. L. Dharani, Dr. B. Armaly, Dr. X. Du, Dr. C. Wang and Dr. Vy Khoi Le, for the time and advice they provided when reviewing my dissertation.

I must also thank my research group members. I would never have been able to finish my dissertation without them.

I would like to express my gratitude to the Department of Mechanical and Aerospace Engineering at Missouri University of Science and Technology. My graduate research assistantship within this department provided me with financial support during my academic studies.

I am grateful for my two older brothers, my younger sister and my younger brother. They offered continuous support and encouragement. Finally, I would like to thank my wife. She always believed in me and helped me during my study.

**TABLE OF CONTENTS**

## LIST OF ILLUSTRATIONS

**Paper III**

# LIST OF TABLES

## 1- INTRODUCTION

A composite material is created when two or more materials are combined into one, often containing very different properties. This combination produces a composite that has unique properties. The different materials can, however, be easily distinguished from one another neither nor a blend into one another. The constituent materials in the composite include fibers and a matrix. Fiber reinforcements are the major load carrying components. Polymer matrix is used for the load transfer as well as barrier against adverse environments between the fibers. Composites are currently being considered as an alternative to conventional materials such as, aluminum and steel, due to their high specific strength, high specific modulus, and corrosion and wear resistance.

Fiber-reinforced polymer composites are increasingly being used in various applications (aerospace, marine, and automotive) because they have low weight, a high stiffness, a high strength, a superior fracture behavior, and a long service life. They are also highly resistant to corrosion. Several types of fiber reinforcements exist for fiber-reinforced polymer composites. Glass fibers however, are used most often [1]. Glass fibers have gained popularity because they are more readily available and cost effective than carbon either aramid fibers. Glass fiber-reinforced polymer composites have a number of applications including, aircraft gliders, boats, automobiles, wind turbines, storage tanks, piping, bridge decks, and houses. Several types of thermosetting polymer resins are used as a matrix to bind the reinforcement material. Polyurethane (PU) is a thermoset resin which is more environmentally friendly. Unlike conventional resin systems (polyester and vinyl Ester) [2-5]. PUs do not contain volatile organic compounds (VOC)-emitting styrene and peroxide catalysts. A PU resin system typically contains both isocyanates and polyols. PU resin is inexpensive. It also has a high processability, a high impact resistance, and superior mechanical properties. These qualities make it an attractive alternative to other resin systems. Pultrusion is used to conventionally manufacture glass fiber-reinforced PU composites. Pultrusion is limited, however, to manufacturing constant cross-section profile composite parts. The Vacuum Assisted

Resin Transfer Molding (VARTM) process is a low cost composite manufacturing process that is widely used in the composite industry. This process was developed over the last two decades for applications in commercial, military, and marine composite structures [6, 7]. Virtually any size part can be manufactured at low pressures and temperatures using VARTM process. Manufacturing of glass fiber-reinforced PU composites using VARTM process is new. As a result, few have investigated it. Tate et al. [8-10] used VARTM process to manufacture E-glass/soy-based PU composites and nano-modified E-glass/soy-based PU composites. The authors have used a two-part PU resin system in the manufacturing process and the mechanical properties of E-glass/soy-based PU composite were compared with E-glass/vinylester and E-glass/polyester composites. The mechanical properties of the E-glass/soy-based PU composites were comparable to both the E-glass/vinylester and the E-glass/polyester composites. The damage resulting in composite materials from impacts load cannot always be detected by visual inspection. This damage can range from barely detectable to matrix cracking, fiber failure, and delamination. A large body of literature addresses damage mechanisms, damage detection methods, and the numerical simulations of damage progression in composites. Zhang et al. [11] used ABAQUS TO perform a series of finite element analyses. The authors predicted both damage initiation and propagation in laminated carbon/epoxy composite plates that were subjected to low-velocity impacts. Aslan et al. [12] conducted not only an experimental study. But also numerical simulations to investigate the in-plane dimension effect on the impact response of cross-ply glass/epoxy laminated composite plates under low-velocity impact. They found that the impact behavior of composite structures is directly dependent on the in-plane dimensions. Tiberkak et al. [13] developed a finite element model based on Mindlin's plate theory to study the low velocity impact behavior in fiber-reinforced composite plates. Shi et al. [14] implemented cohesive damage in their finite element model and studied the low velocity impact of a composite laminate. The authors have inserted interface cohesive elements between plies with appropriate mixed-mode damage laws to model delamination. The numerical results were in good agreement when compared to experimentally obtained curves of impact force and absorbed energy versus time. The

simulation results showed a good correlation with experimental data in terms of both force displacement curves and material damage. Fan et al. [15] developed a finite element model to predict the impact behavior of the woven glass fiber-reinforced composite plates. Hashin failure criteria was used to study the damage that occurred in the composite plate. The authors have observed that the perforation energy increased as the thickness increased. Both the material and the damage behavior of theses composites must be understood if an optimum performance is to be achieved.

## 2- SCOPE OF THE DISSERTATION

Composite materials have replaced metals in various engineering applications as result of their numerous advantages in mechanical properties as well as reduced cost while selecting the material systems for typical application [1]. A thorough understanding of the material behavior of these composites is necessary to achieve optimum performance [2]. Analyzing the neat resin properties in addition to the composite behavior is significant to assess the overall performance of composite. Mechanical properties of neat resins are important to study because this can be attributed to the initial damage in the composite material which primarily occurs through matrix cracking [3].

Polyurethane (PU) is better and a promising alternative to polyester and vinylester as it offers the potential for fast cycle times, high toughness. There is no styrene emission during PU VARTM processes and the final product has superior durability. For two part resins after mixing, the urethane system begins to react and the viscosity increases, delaying the infusion of the resin into large parts. Viscosity and pot-life limitations of PU resins have been overcome through a major development in novel catalysis chemistry. This dual catalyst system extends the pot-life of mixed resins at room temperature with a tunable induction period and a snap-cure profile at high temperatures [4]. In particular this chemistry offers the following advantages:

• Lower resin viscosity compared to epoxy resins which facilitate easy fabrication of composite part.

• Longer pot-life compared to commercial urethane-based resins.

• A reduction in cycle time which is achieved by a snap-cure mechanism.

• Higher mechanical performance compared to commercial urethane resins, fracture toughness in particular.

• Good thermal stability, excellent fire performance without added flame retardants, low smoke density and less toxicity according to NF P52-901 standard [5-6].

Recent advancements in PU chemistry for vacuum assisted resin transfer molding VARTM and Resin Transfer Molding (RTM) processes have resulted in a dramatic

increase in commercial interest for producing a wide range of products, including those utilized in wind energy production.

Glass fiber-reinforced PU composites are conventionally manufactured using pultrusion. However, pultrusion is limited to manufacturing of constant cross-section profile composite parts. Vacuum Assisted Resin Transfer Molding (VARTM) process is a low cost composite manufacturing process and widely used in composite industry. The major challenge is in using PU resin system for vacuum infusion processes VARTM in maintaining a relatively constant, low viscosity for a long period of time. Also, the isocyanate portion of the reacting components tends to react with water to produce carbon dioxide, which results in foaming. VARTM process has advantages over conventional Resin Transfer Mold (RTM) by eliminating the costs associated with matched-metal mold making and volatiles emission. In VARTM process, the polymer resin is infused through the fiber reinforcements under atmospheric pressure.

The focus of the present work in Paper I is Synthesis and Performance Evaluation of Polyurethane Composites using One-part and Two-part VARTM Resin Systems. Two types of PU resin systems, PU 90IK01 and PU 840871, were used for manufacturing the composite laminates. Six layers of glass fiber were used for impact and flexure specimens and three layers glass fiber for tension specimens with thermoset PU 90IK01 and PU 840871 resin systems. Thermal studies of both the resins were conducted using differential scanning calorimetry (DSC) and viscosity measurement. Tensile and flexure tests are conducted on both the neat resin and glass fiber reinforced PU composite laminates. Also low velocity impact tests are performed on the two types of glass fiber reinforced PU composite laminates.

In paper II: Manufacturing and Characterization of Polyurethane Based Composite Bridge Deck Panels using VARTM Process. Three different models of all-fiber reinforced polymer composite sandwich bridge decks utilizing various core designs, namely box, trapezoid and polyurethane (PU) rigid foam, were fabricated using VARTM process. The three models are evaluated mechanically Flexural, flatwise compression and edgewise compression tests and compared in order to choose the appropriate design for

full scale bridge decks. Woven glass fiber and two part thermoset polyurethane resin systems were used for fabrication. In ddition, finite element analysis were conducted using software ABAQUS to model the flexural results for the trapezoid foam model.

In paper III: Design and Manufacturing Composite Structural Insulated Panels (CSIP) for Modular House Construction. Usage of glass fiber reinforced two-part PU composite to Design and manufacture composite structure insulation panels. To meet housing core challenges, innovative processing techniques combined with new materials technology will be developed and evaluated. The core-filled manufacturing process will be modified to manufacture multifunctional panels for housing and army shelter applications, the core-filled composite panels are lightweight and easy to transport. Energy efficiency is inherent with the core-filled composite panel than in a metallic material. A series of tests like flexure, compression, weathering, and UV resistant will be performed on these structural components.

**PAPER**

# I. MANUFACTURING AND PERFORMANCE EVALUATION OF POLYURETHANE COMPOSITES USING ONE-PART AND TWO-PART RESIN SYSTEMS

M. Mohamed, S. Hawkins and K. Chandrashekhara
*Department of Mechanical and Aerospace Engineering*
*Missouri University of Science and Technology, Rolla, MO 65409*

## ABSTRACT

Polyurethane (PU) based composites show superior performance compared to polyester and vinylester based composites. The demand for PU composites is increasing in high technology as well as conventional applications such as infrastructure and automobile. In this study, Glass fiber reinforced composite laminates using one-part and two-part PU resin are manufactured using vacuum assisted resin transfer molding (VARTM) process. A new generation of two-part thermoset PU resin system is investigated and compared with commercial one-part PU resin systems. The mechanical performance of glass fiber reinforced composites manufactured using two different PU resin systems is evaluated. Tensile and flexure tests are conducted on both neat resin and glass/PU composites. Low velocity impact tests are performed on the two types of glass fiber reinforced PU composite specimens. Mechanical properties including strength and modulus were measured and analyzed for the two resin systems. Differential scanning calorimetry (DSC) is used to study the cure behavior of both resin systems. A Brookfield LVDV-II programmable rotational type viscometer is employed to study the viscosity profiles of the resin systems. The influence of resin properties on the overall performance of glass fiber reinforced composites is discussed.

## 1-INTRODUCTION

Composite materials are advantageous over metals in various engineering applications due to advantages like high specific stiffness, high specific strength, enhanced dimensional stability, energy absorption, corrosive resistance as well as reduced cost with selected material systems for typical application [1-2]. However, a thorough understanding of the material behavior of these composites is necessary to achieve optimum performance [3]. Analyzing the neat resin properties in addition to the composite behavior is necessary to assess the overall performance of the composite. Mechanical properties of neat resins are important to study because this can contribute to the initial damage in the composite material which is primarily due to matrix cracking [4].

Polyurethane (PU) is a better and promising alternative to polyester and vinylester as it offers the potential in terms of fast cycle times and high toughness. There is no styrene emission during PU VARTM processes and the final product has superior durability [5]. For two-part resins, the urethane system begins to react after mixing and the viscosity increases, constraining the infusion of the resin into large parts. Novel catalysis chemistry is used to overcome the viscosity and pot-life limitations of PU resins. This dual catalyst system extends the pot-life of mixed resins at room temperature with a tunable induction period and a snap-cure profile at high temperatures [6]. This chemistry offers the following advantages:

- Lower resin viscosity compared to epoxy resins and facilitate easy fabrication of composite part.
- Longer pot-life compared to commercial urethane-based resins.
- A reduction in cycle time through a snap-cure mechanism.
- Higher mechanical performance compared to commercial urethane resins, fracture toughness in particular.
- Good thermal stability, excellent fire performance without added flame retardants, lower smoke density and less toxicity according to NF P52-901 standard [7-11].

Recent advancements in PU chemistry for vacuum assisted resin transfer molding (VARTM) and Resin Transfer Molding (RTM) processes have leaded to a dramatic increase in commercial interest for producing a wide range of composite products, including those utilized in wind energy production. The major challenge is moisture sensitivity while using PU resin system for vacuum infusion processes. The isocyanate portion of the reacting components tends to react with water to produce carbon dioxide, which results in foaming [12]. VARTM process is one of the most widely used composite manufacturing processes developed in recent years for several engineering applications. VARTM process has advantages over conventional Resin Transfer Mold (RTM) by eliminating the costs associated with matched-metal mold making and volatiles emission. In VARTM process, the polymer resin is infused through the fiber reinforcements under atmospheric pressure.

Not many researchers have investigated the behavior of PU composites manufactured with VARTM process. Michael et al. [11] investigated the physical and mechanical properties of pultruded PU composites, and compared them to unsaturated polyesters (UPE), vinylester (VE) and hybrid unsaturated polyester-urethane (UPE-PU) resin profiles with identical reinforcements. The authors observed PU pultruded composites to exhibit superior strength and toughness compared to VE, UPE and hybrid UPE-PU based composites.. Husic et al. [9] studied and compared the mechanical properties of untreated E-glass fiber reinforced composites prepared with soybean oil-based PU to the petrochemical polyol based ones. The results showed that soy-based PU offers better mechanical properties

Usama [10] investigated the chemistry and properties of the PU material, with emphasis on structure/property relationship and the development of high surface quality (Class A) VARTM composites. The author has also discussed the advantages of PU resins including room temperature cure, no volatile organic compounds (VOCs) and high impact properties. The results showed that PU chemistry for use in RTM and vacuum infusion applications are an attractive alternative to other materials. Usama and Srekan [13] have studied the new generation of PU resin systems developed by Bayer

MaterialScience. The study focused upon the performance of a new PU resin system versus traditional epoxy and vinylester resins used for wind blades and investigated the effects of carbon nanotubes on the performance of PU. These urethane systems showed improved fatigue and fracture toughness properties as well as faster de-mold times than other resins.

In this study, glass fiber reinforced PU composite laminates are fabricated using VARTM process. Two types of PU resin systems, PU 90IK01 and new generation PU 840871, are used for manufacturing the composite laminates. Thermal studies of both resins were conducted using differential scanning calorimetry (DSC) and viscosity measurement. Tensile and flexure tests are conducted on both the neat resin and glass fiber reinforced PU composite laminates. Low velocity impact tests are performed on both types of glass fiber reinforced PU composite laminates. In the previous study by the same author, Mohaned [5] has investigated the impact characterization of PU one-part composites manufactured with VARTM process experimentally and numerically using finite element analysis. The results showed that PU composites manufactured using thermoset PU resins and VARTM process have good mechanical properties such as tensile strength, flexural strength, tensile modulus and flexural modulus.

## 2- MATERIALS AND MANUFACTURING

Woven fiber based composites offer improved performance over unidirectional type composites. The woven fiber structure provides obstruction to matrix splitting and delamination growth [14]. In this work, woven E-glass fibers which are compatible with PU resins are used obtained from Owens Corning Inc. OH.

Two types of PU resin systems compatible with VARTM are obtained from Bayer MaterialScience, PA. The two PU resin systems investigated in this study are a two-part RTM NB# 840871 resin system and a one-part PU 901K01 resin system. These resin systems possess better manufacturing feasibility. Table 1 shows the typical impact properties of PU resin system when compared to conventional resin systems, such as polyester and vinyl ester. The two-part PU with a trade name of RTM NB# 840871

comes in two separate parts which will react once combined. The "A" component is an Isocyanate NB#840859 ISO, Diphenylmethane diisocyanate (MDI- Aromatic) and the "B" component is a Polyol RTM NB#840871. The mix ratio by weight for the A and B components is 92:100. These two components are referred to as a PU 840871 resin system in the rest of the paper. One-component Blendur PU 901K01 is a modified polyisocyanurate casting resin based on Diphenylmethane Diisocyanate (MDI). The casting resin reacts on heating without the addition of a catalyst to from a crosslinked thermoset with excellent thermal stability.

## 3- EXPERIMENTS

### 3.1 Preparation of PU Neat Resin Tensile and Flexure Samples using Blendur® TP.PU90IK01 and PU840871

Eighteen tensile and flexure samples were manufactured using Blendur® TP PU 90IK01 one-part thermoset resin system and PU 840871 two-part thermoset resin system. The resin was degassed under vacuum to remove dissolved air. The one-part resin system, PU90IK01, was heated to 50°C to reduce the viscosity such that it can be easily filled into the mold. All the moisture content was removed from the aluminum mold by heating for 2 hours at 250°C before the measured quantity of the resin was poured into the mold. The curing cycles were 200°C for 3 hours for PU 90IK01. A 70°C hold for 1 hour and 80°C for 4 hours for PU 840871, as manufacturer recommended.

### 3.2 Manufacturing Composite Specimens

Vacuum Assisted Resin Transfer Molding (VARTM) process was utilized to manufacture the composite laminates. Five panels 10 in. x 10 in. are manufactured for each resin system. To test the mechanical properties of the composite laminates, specimens are cut from the panels manufactured. Fiber reinforcement layup is prepared on a rigid aluminum mold with a layer of removable plastic flow-enhancement medium (to reduce fill time) along with peel ply (to facilitate easy removal of manufactured part). The layup is sealed using a vacuum bag. The whole setup is then sealed to the rigid mold using a bagging tape. The layup is infused at 50 °C and cured at 28 in. of Hg vacuum

pressure at 200$^o$C and held for 3 hours for one-part resin system. For the two-part resin system, the infusion was at room temperature and the curing cycle was 70 $^o$C for 1 hour and 80 $^o$C for 4 hours. Standard coupon tests were conducted including tension, flexure, and low velocity impact as per ASTM standards. Both Differential Scanning Calorimetry (DSC) and viscosity measurement tests were conducted on neat resin samples.

Tensile specimens were manufactured using three layers of woven E-glass for tensile test, and impact and flexure specimens were manufactured with six layers. By using six layers in the tensile test the samples were thick and the failure occurred in the grips was not acceptable. The thickness was reduced to three layers for the tensile test and the failure occurred in the middle of the samples between the upper and lower grips.

### 3.3 Tensile Test

Tensile tests were performed on both the neat resin and composite laminate specimens according to ASTM D638-10 and D3039/D3039M-08, respectively, [15, 16]. The composite specimens measured 250 mm x 25.4 mm (10 in. x 1 in.). The specimens' end tabs were produced from the same glass fiber and PU resin, to protect against the gripping stress produced from the tensile testing machine fixture. The tests were performed on an Instron 5985 test machine with load cell 250 kN for composites specimens and 10 kN for neat resin specimens. Ten glass fiber/PU 90IK01 and ten glass fiber/PU 840871 specimens were tested.

### 3.4 Flexure Test

Flexure experiments were performed on both the neat resin and the composite laminate specimens according to ASTM standard (D790-10) [17]. Nine samples were manufactured for neat resin and ten samples for composite laminate specimens with dimensions of 127 mm x 12.7 mm x 3 mm (5 in. x 0.5 in. x 0.118 in.). These tests were performed on an Instron 4469 electro-mechanical UTM machine at a crosshead speed of 0.06 in/min.

### 3.5 Impact Test

Low velocity impact tests were performed on a Dynatup Instron Model 9250 Impact Testing machine with impulse control and data system. At the beginning of the test, impactor was secured with a hook at the desired height. When the release mechanism was activated, the impactor was allowed to free-fall under gravity. The drop height was varied as per the required impact energy by adjusting the position of the impactor. The position was measured with either a meter stick or a tape measure. A 12.7 mm (0.5 in.) hemispherical hardened steel tup of mass 6.5 kg was connected to the drop tower impactor. During the low velocity impact tests, the specimens were clamped in a fixture concentric with the axis of a drop tower passing through the tup. The low velocity impact test fixture was made of steel, with a 44.45 mm x 44.45 mm (1.75 in. x 1.75 in.) opening to ensure that the test specimens remained clamped along all four edges. Experiments were conducted at three different energy levels, 10J, 20J and 30J.

## 4- RESULTS AND DISCUSSION

### 4.1 Differential Scanning Calorimetry

Differential Scanning Calorimetry (DSC) is an experimental tool used extensively for thermal property analysis. It works by detecting heat flow from the samples as a function of time. DSC is used to characterize cure kinetics for thermosetting polymer resins. The heat of reaction, the rate of cure, and the degree of cure can be measured using a DSC. In this work, a Model 2010 DSC was used to study the cure kinetics from two formulations of polyurethane resins. Resin samples weighing 5-10 mg were encapsulated in an aluminum pans. Dynamic runs at a heating rate of 5°C/min were conducted to determine the maximum heat reaction temperature during the curing cycle from the two PU formulations, as shown in Figure 1. The 5-10 mg resin samples were placed in the DSC furnace at ambient temperature. They were cooled rapidly to -35°C under liquid nitrogen. The exothermal was then monitored from -35°C to 200°C for PU 90IK01 and from -35°C to 175°C for PU 840871 with same heating rate 5°C/min to determine the glass-transition temperature ($T_g$).

The glass transition temperature Tg is one of the most important properties of any polymer and is the temperature region where the polymer transitions from a hard, glassy material to a soft, rubbery material. As PU are thermosetting materials and chemically cross-link during the curing process, the final cured PU material does not melt or flow when reheated (unlike thermoplastic materials), but experiences a slight softening (phase change) at high temperatures. The ultimate Tg is determined by a number of factors: the chemical structure of the PU resin, the type of hardener and the degree of cure. After the PU passes through the glass transition temperature range, its material properties change significantly. It is important that design engineers understand the nature of this transition, so that they can choose the best system for a specific application.

The glass-transition temperature is reported as the midpoint temperature of the extrapolated endothermic shifts observed during the re-scans. The glass-transition temperatures of the two PU resins were observed to be significantly different. The $T_g$ for PU90IK01 was found to be 122.38°C and 70.84°C for PU840871 as seen in Figure 2. The reason why Tg of one-part PU 90IK01 is higher is that it contains a large number of aromatic rings (Figure 3), which decreases the free volume in the PU polymer. The results are shown in Table 2.

**4.2 Viscosity Measurements**

A Brookfield LVDV-II programmable rotational type viscometer was used to obtain rheological measurements on thermosetting resins. A dynamic viscosity measurement was utilized to determine the optimum infusion temperature. A Brookfield LVDV-II programmable rotational-type viscometer was used to perform the viscosity measurements. The viscous resistance is related to both the spindle rotational speed and the spindle geometry. For both the PU 90IK01 and PU 840871, the spindle number SC4-18 was used with a speed of 0.30 RPM and 5.0 RPM, respectively, and the chamber used is 13R. The resin sample temperature was controlled with a hot water bath. The thermocouple attached to the chamber to measures the real-time temperature of the resin in the chamber, providing feedback to the temperature controller.

Brookfield viscometers constructed generally consisted of a chamber (outer cylinder) attached to the instrument and a spindle (inner cylinder) driven at a constant speed (Figure 4). Pour some resin sample in the chamber and the spindle is immersed in the resin and rotates at a constant speed around its central axis. The spindle will experience a retarding force due to the viscous drag of the resin. The torque transmitted through the liquid to a static outer cylinder the more viscous the sample, the more torque required to rotate the spindle. Thus, a constant shear stress is applied on the cylinders. The speed being inversely proportional to the distance between the two cylinders. There are no mechanical devices attached to the spindle, so that all frictional dissipation of energy occurs in the liquid itself.

The accuracy of calculated average shear stresses for this viscometer should also be examined. Thus, the rotational speed, measured torque, and consideration of the spindle size and shape allow us to determine shear rate and shear stress using equations below:

$$\dot{\gamma} = r\frac{d}{dr}(\frac{V_\theta}{r}) = \frac{-2\omega r_1^2 r_2^2}{r^2}(\frac{1}{r_2^2 - r_1^2})$$

$$T = F \times r_1$$
$$\tau_{r\theta}\big|_{r=r_1} = \frac{T}{2\pi r_1^2 L}$$

The ratio of shear stress and shear rate are given us the apparent viscosity η.

$$\eta = \frac{\tau}{\dot{\gamma}}$$

$$\eta = \frac{T}{\omega}\frac{1}{4\pi L}\frac{r_1^2 - r_2^2}{r_1^2 r_2^2}$$

Where $\gamma$ is the shear rate, $\tau$ is the shear stress, $\omega$ is the angular velocity (RPM), T is the torque, $r_1$ is the radius of the spindle (inner cylinder), $r_2$ is the radius of the chamber (outer cylinder), r is a radius at any point between the two cylinders and L is the spindle length. In practice, these constant factors and measured variables are used by computer software to calculate viscosity.

The viscosity of the PU 90IK01 resin was found to be 5.5 times greater than that of the PU 840871 resin at room temperature due to the length of the chemical chain and good entanglement between the molecules at room temperature as shown in Figures 3, 5 and 6. However, when both resins are heated, the PU 90IK01 resin becomes less viscous than the PU 840871 due to the faster gel time of the PU 840871 resin. The viscosity of the PU 90IK01 dropped from 2053 cPs at room temperature to 33 cPs at 89°C.  For the PU 840871, the viscosity dropped from 357 cPs at room temperature to 352 cPs at 33°C. The viscosity had then increased due to the resin's low pot life resulted of the catalyst part (Isocyanate) which start react directly after mixing at room temperature, on the contrary one-part PU 90IK01 which start reacting at certain temperature due to the thermal stability and high heat distortion temperature. The results were agreed with finding by U. Younes .The measured viscosity of both PU 90IK01 and PU 840871 at various temperatures is given in Tables 3 and 4, respectively.

## 4.3 Tensile and Flexure Testing

Figure 7 illustrates the average tensile stress-strain behavior of the PU 90IK01 and PU 840871 neat resin specimens at a crosshead speed of 0.06 in/min; between the two resin systems, there was a significant difference in the maximum stress needed to cause failure. In the case of PU 90IK01 resin, had no plastic deformation range causing it to fail abruptly and fracture was observed at a much lower stress. This resin was observed to be more brittle than the PU 840871 resin because it contains large numbers of hydroxyl group (OH) and the benzene rings in the chemical structure which make the chain stiffer. In contrast The PU 840781 was able to endure 54% higher stress and 0.027 % higher strain and fails gradually. Figure 8 shows the average flexure stress-strain

behaviors of the PU 90IK01 and PU 840871 neat resin specimens. The stress-strain behavior displayed an increase in the region of linear elasticity with increasing strain. The ductility property of two part resin PU 840871 it's appear again and a significant difference exists between the two resin systems, in the maximum stress needed to cause failure. In case of the PU 90IK01 resin, fracture occurred at the yield stress. It proved to be more brittle than the PU 840871 resin, causing fracture at a much lower stress. The PU 840871 specimen was able to handle 39% more flexural stress and more strain (Table 5).

Figure 9 illustrates the average tensile stress-strain behavior of the glass fiber/PU90IK01 and glass fiber/PU840871 composite specimens. A linear relationship is clearly visible between stress and strain. Since the tensile property is fiber domain and in this work same type of fiber was used therefore, cannot see much difference in the tensile strength. However, some of the characteristics of the neat resins can be seen in the composites. The brittle nature of the PU 90IK01 resin does not allow the composite to reach either the same load or extension as the other resin. Both composites demonstrated a linear elastic behavior, but lack a plastic deformation range making the yield stress the breaking point. Fracture occurred at the yield stress for glass fiber/PU840871 at higher tensile strength than the glass fiber/PU90IK01 composites. Also, there is difference in the failure modes of the specimens. The glass fiber/PU840871 specimens failed laterally and the glass fiber/PU90IK01 specimens failed by splaying of the fibers as shown in Figure 10.

Estimates of tensile strength were based on both the stress at linear elastic limit and the maximum stress levels. Results show no significant change in maximum strain in the case of specimens belonging to PU 840871 resin and the average strain was 0.024% at the maximum stress 350 MPa which is slightly higher than 300 MPa in case of PU 90IK01.

Figure 11 illustrates the average flexure stress-strain behavior of the glass fiber/PU 90IK01and glass fiber/PU840871 composite specimens. Figure 11 indicates that the composite specimens take on some characteristics of their respective matrix. The neat resin flexure test in Figure 8 infers that the PU840871 resin had better properties than the

PU 90IK01. Even though the glass fiber/PU840871 composite was able to handle a slightly higher strain, the glass fiber/ PU840871 composite could handle a higher stress of 642 MPa (Table 6).

## 4.4 Impact Test

In this study, the effects of three different impact energies (10J, 20J, 30J) on the maximum contact force, maximum deflection, contact time and absorbed energy of the glass fiber reinforced PU 90IK01 and glass fiber reinforced PU 840871 laminated composite were investigated.

Front face for two type composite specimens subjected to impact energy at 10J initially there was slight damage at the front face crossovers under the impact head. Then fiber damage occurred at the center, aggravated and then increases by increasing the energy levels. Finally shear failure of the fibers occurred as the impact head hit the specimen. A circular area of delamination centered under the impact head formed with increasing impact energy. In the back face of the specimens at 10J the damage barely visible, at 20J and 30J at the center was a rough diamond shaped area of matrix cracking within the fiber bundles. This damage extent and matrix damage started, followed by fiber damage.

The percentage of the impact damage absorbed by the Glass fiber/PU 90IK01 specimen increases with impact energy. It can be seen that the force varies fairly broad peak with time, however, at higher energies the peak becomes sharper as damage occurs under the impactor. Again, there was a fair degree of damage even in the specimens subjected to the lowest energy impacts. The same styles as for the Glass fiber/PU 840871 specimens were seen, but generally buckling of the surfaces occur at high energy level. Total perforation of the specimens subjected to the highest energies did not occur. Figures 12 and 13 show the damaged areas obtained by visual inspection for both composite laminates.

As expected, the Glass fiber/PU 90IK01 specimens are stiffer than Glass fiber/PU 840871. For the Glass fiber/PU 90IK01 specimens at higher impact energies, a sharp

increase of maximum defection is seen as partial perforation of some of the specimens occurs. Again the higher stiffness of the Glass fiber/PU specimens can be seen in Figure 14 through the higher forces comes across. For the maximum deflection, maximum force and absorbed energy plots, no obvious difference was seen between different composite laminates. However, the Glass fiber/PU840871 has slightly higher energy absorption.

Flexible plates Glass fiber/PU840871 give high bending strains that lead to compressive and/or tensile failure on the faces of the plate. Stiffer plates lead to higher contact forces and internal shear and normal stresses give complex inter laminar and matrix damage modes. The use of a hemispherical impactor even for small energy level and forces a smaller contact area occurs, leading to higher shear and normal stresses. Close to the impactor a first approximation leads to a circular region of high shear stress around the circumference of the area of contact. This leads to delamination that spreads inwards faster than outwards [18]. In reality the stress under the impactor is complex. From the results In-plane stresses cause transverse matrix tensile cracks which can cause delamination. These cracks are important in a marine and infrastructure applications due to the problems of material property degradation through moisture diffusion.

Table 7 gives the low velocity impact response of the two laminates. At 10J, the contact force was approximately the same for both composite laminates. Figure 14 illustrates the load versus time curves at three different energy levels. Additional delaminations were observed as the impact energy increased. The glass fiber/PU90IK01 composite carried approximately 13% more load at the 30J energy level than the glass fiber/PU840871 composite. From Figure 14, the maximum load was 8000 N for both the 20 J and 30 J energy levels in the PU 840871 composite. This is mainly due to the flexibility of the PU 840871 resin.

Figure 15 illustrates the variation of impact energy with respect to time. An initial increase in the impact energy (in the curves) relates to the transfer of energy from the drop weight to the composite sample. A downward trajectory and a consecutive plateau in the curve depict the transfer of energy from the sample to the impactor and final energy absorbed by the sample, respectively. The energy absorption was slightly higher

in the glass fiber//PU840871 composite. Figure 16 illustrates the load versus deflection behaviors of both the composite specimens at three energy levels. The effect of load on the deflection is significantly increased with increasing energy levels.

## 5- CONCLUSIONS

In this study, glass fiber reinforced composite laminates were fabricated using VARTM process. Thermoset polyurethane PU 90IK01 and new generation PU 840871 resin systems, and bi-directional E-glass fabric was used as the reinforcing material. Differential Scanning Calorimetry (DSC) and viscosity measurement was used to study the properties of the two PU resin systems. A performance evaluation was conducted using tensile, flexure, and low velocity impact tests at three different energy levels (10J, 20J and 30J), for each resin system and the results were compared to each other.

DSC tests were performed to investigate and obtain the glass transition temperature $T_g$ for both PU resin systems. Dynamic viscosity measurement was utilized to determine the optimum infusion temperature for both resin systems and the results are agreed with results found by Usam. From the tensile test of the neat resin samples, PU 90IK01 was observed to be breakdown fast due to its brittle nature. The PU840871 resin can carry a load 2.5 times greater than that the PU 90IK01can carry. The neat PU 840781 samples were capable of enduring about 54% higher stress and 0.027 % higher strain. The flexure stress-strain behavior showed increasing in the region of linear elasticity, which has higher strength. The PU 90IK01 resin was more brittle compared to PU 840871 resin allowing it to fracture at a much lower stress. The PU 840871 neat resin specimen was able to handle 39% more flexural stress and more strain. The brittle nature of PU 90IK01 resin does not allow the composite to reach either the same load or extension as the other. The PU 840871 resin had absorbed more energy than PU 90IK01.

Summarizing the results in terms of mechanical properties the resin system PU 840871 laminates outperformed the PU 90IK01glass fiber laminates in all respects except

the contact force in the low velocity impact test. Both composites exhibit excellent properties and are considered suitable for use in infrastructure and marine applications.

## 6- ACKNOWLEDGMENT

# 7- REFERENCES

[1] K. S. Pandya, C. Veerraju, and N.K. Naik, "Hybrid Composites made of Carbon and Glass Woven Fabrics under Quasi-Static Loading." Materials and Design, Vol. 32, pp. 4094-4099, 2011.

[2] L. Hammond and R. Grzebieta, "Structural Response of Submerged Airbacked Plates by Experimental and Numerical Analyses." Shock Vibration, Vol. 7, pp. 333-341, 2000.

[3] C. Wonderly, J. Grenestedt, F. Goran, and E. Cepus, "Comparison of Mechanical Properties of Glass Fiber/Vinyl Ester and Carbon Fiber/Vinyl Ester Composites." Composite Part B: Engineering. Vol. 36,pp. 417-426, 2005.

[4] G.E. Husman, J.M. Whitney, and J.C. Halpin, "Residual Strength Characterization of Laminated Composites Subjected to Impact Loading." Foreign Object Impact Damage to Composites, ASTM STP 568. ASTM 92-113, 1975.

[5] M. Mohamed, R. R. Vuppalapati, S. Hawkins, K. Chandrashekhara, and T.Schuman, "Impact Characterization of Polyurethane Composites Manufactured using Vacuum Assisted Resin Transfer Molding." International Mechanical Engineering Congress & Exposition ASME Houston, pp. 1-8, November 9-15, 2012.

[6] D. Bareis, D. Heberer, and M. Connolly, "Advances in Urethane Composites Resins with Tunable Reaction Times." American Composites Manufacturers Association Ft. Lauderdale, Florida. Huntsman Polyurethanes Auburn Hills, MI, pp. 1-7, February 2-4, 2011.

[7] J. John, M. Bhattacharya, and R.B. Turner, "Characterization of Polyurethane Foams from Soybean Oil." Journal of Applied Polymer Science, Vol. 86, pp. 3097-3107, 2002.

[8] S. Desai, I.M. Thakore, B.D. Sarawade, and S. Devi, "Effect of Polyols and Diisocyanates on Thermo-Mechanical and Morphological Properties of Polyurethanes." European Polymer Journal, Vol. 36, pp. 711-725, 2000.

[9] S. Husic´, I. Javni, and Z. S. Petrovic, "Thermal and Mechanical Properties of Glass Reinforced Soy-Based Polyurethane Composites." Composites Science and Technology, Vol. 65,pp. 19-25, 2005.

[10] U. Younes, "Development of PU-based RTM and VARTM Technology." American Composites Manufacturing Association Las Vegas, Nevada, pp. 1-17, February 9-11,2010.

[11] M. Connolly, J. King, T. Shidaker, and A. Duncan, "Processing and Characterization of PU pultruded Polyurethane Composites." Technical Paper Huntsman International LLC, pp. 1-16, 2006.

[12] M. Dale, B. A. Acha, and L.A. Carlsson, "Low Velocity Impact and Compression after Impact Characterization of Woven Carbon/Vinylester at Dry and Water Saturated Conditions." Composite Structures, Vol. 94, pp.1582-1589, 2012.

[13] U. Younes and S. Unal, "New Generation Polyurethane-based Fiber Reinforced Composite for Vacuum Infusion and Effect Multi-Walled Carbon Nanotubes on their Performance." American Composites Manufacturing Association Las Vegas, Nevada, pp. 1-14, February 21-23,2011.

[14] R. Karakuzua, E. Erbila, and M. Aktas, "Impact Characterization of Glass/Epoxy Composite Plates: An Experimental and Numerical Study." Composite Part B 41 (2010): 388-395.

[15] ASTM D638-10 Standard Test Method for Tensile Properties of Plastics. ASTM International, 100 Barr Harbor Drive, P.O. Box C700, West Conshohocken, PA 19428-2959 USA.

[16] ASTM D3039/D3039M-08 Standard Test Method for Tensile Properties of Polymer Matrix Composite Materials. ASTM International, 100 Barr Harbor Drive, P.O. Box C700, West Conshohocken, PA 19428-2959 USA.

[17] ASTM D790-10 Standard Test Methods for Flexural Properties of Unreinforced and Reinforced Plastics and Electrical Insulating Materials. ASTM International, 100 Barr Harbor Drive, P.O. Box C700, West Conshohocken, PA, pp. 19428-2959 USA.

[18] G. A. O. Davies and X. Zheng, "Impact damage prediction in carbon composite structures." International Journal of Impact Engineering; Vol. 16, pp. 149-170, 1995.

Table 1 Impact properties of polyurethane and other conventional resins [11]

| ASTM standard, Dynatup D3763 12.55 tup and 2.29 m/sec | | | |
|---|---|---|---|
| 2.54 mm thick, 2 x 300 g/m$^2$ continuous strand mat, ~68 wt % fiberglass | | | |
| **Property** | **Vinylester** | **Unsaturated Polyester** | **Polyurethane** |
| **Maximum Load (N)** | 3260 | 3047 | 4088 |
| **Energy to Max Load (N-m)** | 18.2 | 11.4 | 24.8 |
| **Total Energy (N-m)** | 29.3 | 27.7 | 38.4 |

Table 2 DSC test

| | **On-Set Temperature ($^\circ$C)** | **End-Set Temperature ($^\circ$C)** | **Glass Transition Temperature ($^\circ$C)** |
|---|---|---|---|
| **PU 90IK01** | 128.51 | 141.54 | 122.38 |
| **PU 840871** | 69.48 | 71.27 | 70.84 |

Table 3 Viscosity measurements of PU90IK01

| Viscosity cP | Speed RPM | Torque % | Shear Stress D/cm$^2$ | Shear Rate 1/Sec | Temperature °C |
|---|---|---|---|---|---|
| 2053.56 | 0.03 | 102.65 | 7.53 | 0.37 | 25.00 |
| 1683.64 | 0.30 | 84.24 | 6.18 | 0.37 | 27.00 |
| 733.84 | 0.30 | 36.68 | 2.69 | 0.37 | 35.00 |
| 189.96 | 0.30 | 9.46 | 0.7 | 0.37 | 55.00 |
| 105.98 | 0.30 | 5.30 | 0.39 | 0.37 | 65.00 |
| 41.99 | 0.30 | 2.12 | 0.15 | 0.37 | 85.00 |
| 33.99 | 0.30 | 1.73 | 0.12 | 0.37 | 89.00 |

Table 4 Viscosity measurements of PU840871

| Viscosity cP | Speed RPM | Torque % | Shear Stress D/cm$^2$ | Shear Rate 1/Sec | Temperature °C |
|---|---|---|---|---|---|
| 356.92 | 5.00 | 59.51 | 23.56 | 6.60 | 25.00 |
| 356.92 | 5.00 | 59.49 | 23.56 | 6.60 | 27.00 |
| 355.12 | 5.00 | 59.23 | 23.44 | 6.60 | 29.00 |
| 353.32 | 5.00 | 58.88 | 23.32 | 6.60 | 31.00 |
| 352.12 | 5.00 | 58.69 | 23.24 | 6.60 | 33.00 |
| 353.92 | 5.00 | 58.97 | 23.36 | 6.60 | 35.00 |
| 375.52 | 5.00 | 62.58 | 24.78 | 6.60 | 37.00 |

Table 5 Tensile and flexure testing of PU neat resins

|  | Tensile Strength (MPa) | Tensile Modulus (MPa) | Tensile Failure Strain (%) | Flexural Strength (MPa) | Flexural Modulus (MPa) | Flexure Failure Strain (%) |
|---|---|---|---|---|---|---|
| PU 840871 Neat Resin | 64.47 $\pm$2.0 | 2594.67 $\pm$102.4 | 0.034 $\pm$0.003 | 109.34 $\pm$6.4 | 26.146 $\pm$2.2 | 5.21 $\pm$0.21 |
| PU 90IK01 Neat Resin | 29.02 $\pm$2.4 | 3352.50 $\pm$111.3 | 0.009 $\pm$0.002 | 66.05 $\pm$1.43 | 31.34 $\pm$2.8 | 2.18 $\pm$0.04 |

Table 6 Tensile and flexure testing of glass fiber/PU composites

|  | Tensile Strength (MPa) | Tensile Modulus (MPa) | Tensile Failure Strain (%) | Flexure Strength (MPa) | Flexure Modulus (MPa) | Flexure Failure Strain (%) |
|---|---|---|---|---|---|---|
| PU 840871 Composite | 351.77 $\pm$15.40 | 19,534.08 $\pm$1800 | 0.024 $\pm$0.02 | 642.34 $\pm$ 22 | 14,560.91 $\pm$105 | 4.96 $\pm$0.1 |
| PU 90IK01 Composite | 309.06 $\pm$ 17.83 | 21,430.3 $\pm$ 2.39 | 0.023 $\pm$0.01 | 618.88 $\pm$ 31 | 17,110.6 $\pm$ 210 | 3.82 $\pm$0.1 |

Table 7 Low velocity impact test results

| | E-glass/PU 90IK01 | | | E-glass/PU 840871 | | |
|---|---|---|---|---|---|---|
| **Impact Level** | **10J** | **20J** | **30J** | **10J** | **20J** | **30J** |
| **Contact Force (N)** | 5772.13 | 8075.1 | 9444.6 | 5770.82 | 7554.65 | 8184.17 |
| **Energy Absorbed (J)** | 3.26 | 11.40 | 23.63 | 5.48 | 12.04 | 24.13 |
| **Velocity (m/s)** | 1.75 | 2.48 | 3.05 | 1.80 | 2.68 | 3.15 |
| **Displacement (mm)** | 3.20 | 5.08 | 6.38 | 3.40 | 5.03 | 6.39 |
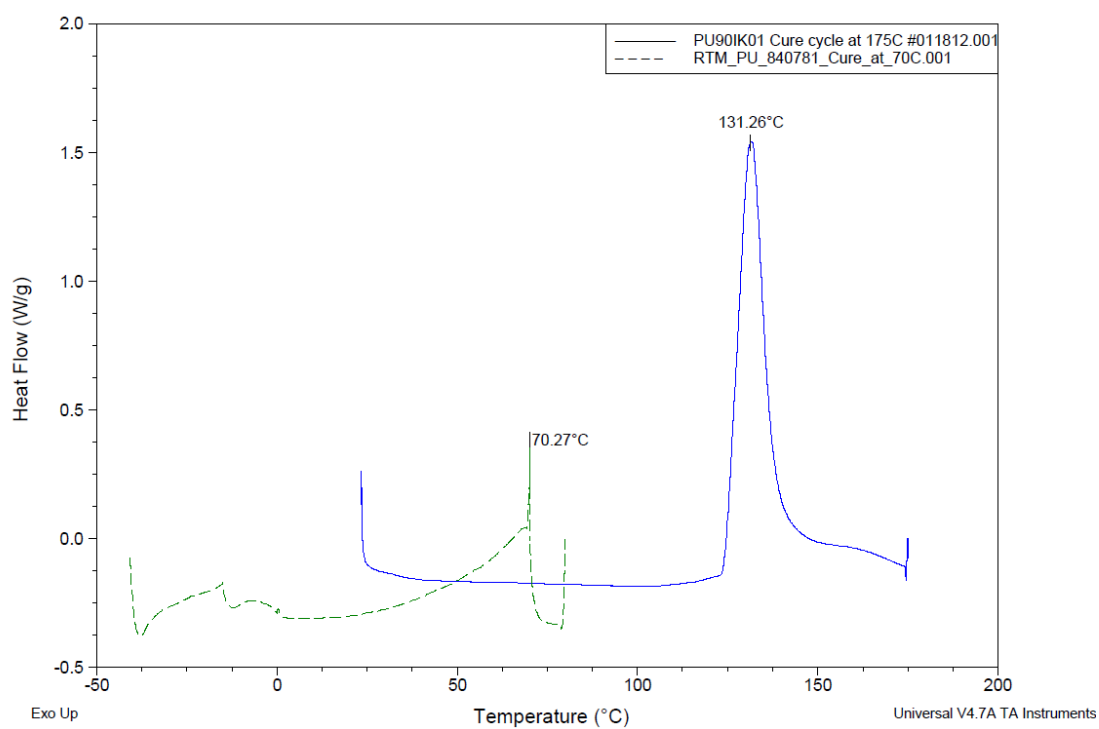
Figure 1 Heat flow vs. temperature at 175°C for PU 840871 and 200°C for PU 90IK01
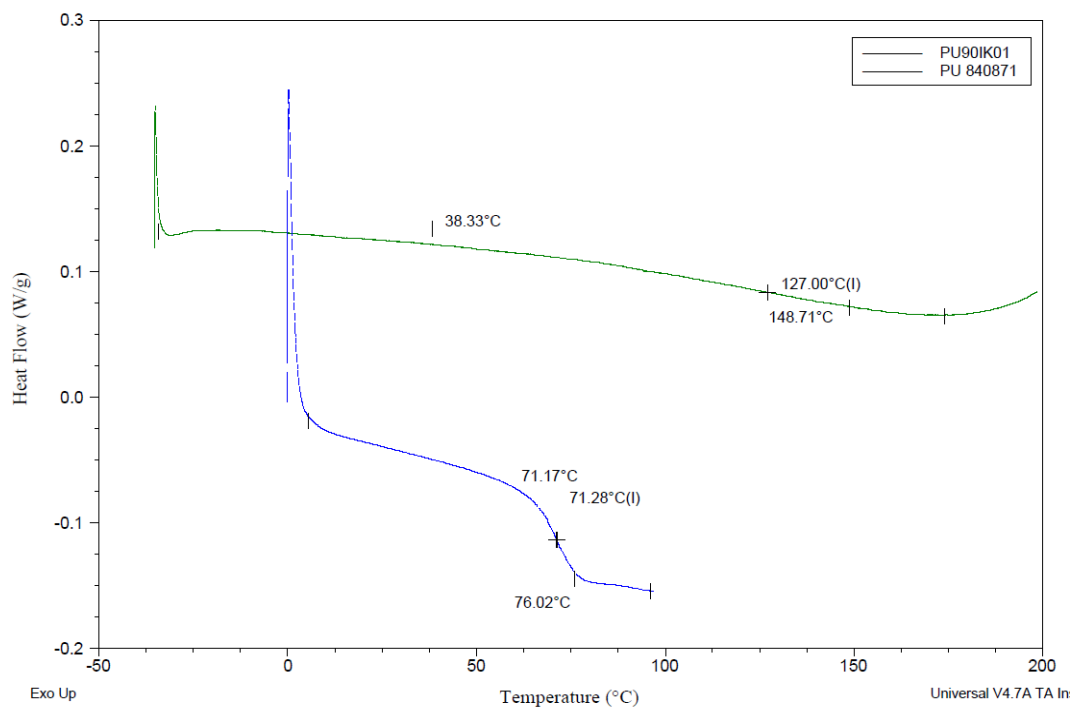
Figure 2 Glass-transition temperature at 175°C for PU 840871 and 200°C for PU 90IK01
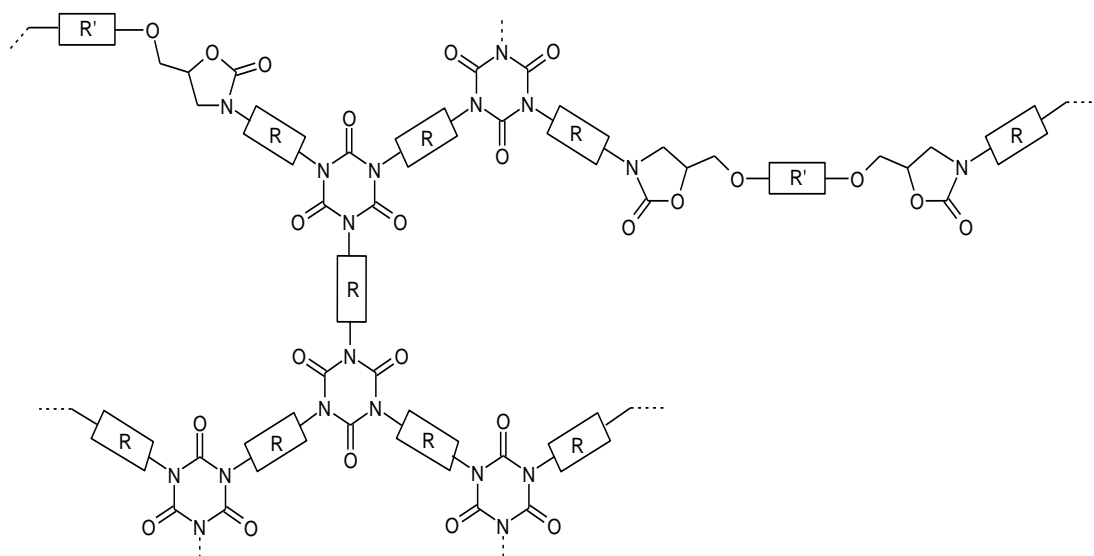


Figure 3 The chemical structure shows the aromatic rings in PU90IK91
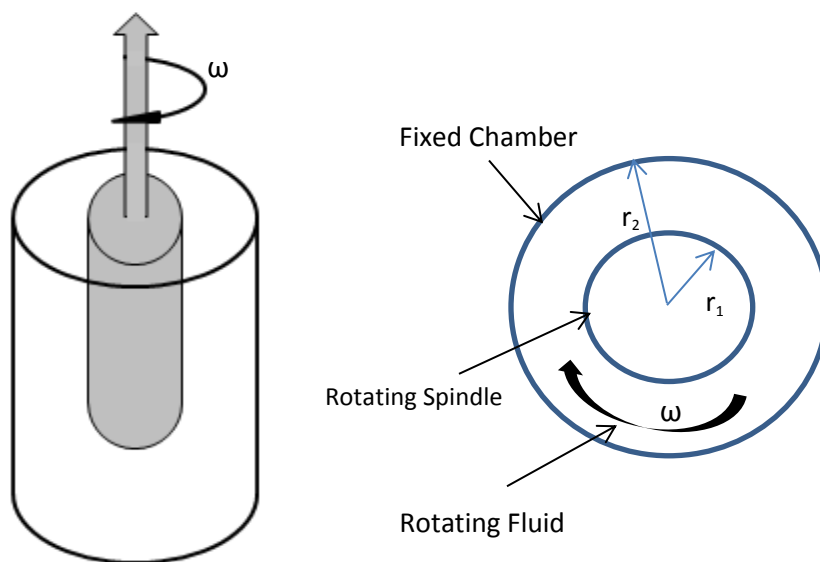
Figure 4 Schematic of rotating spindle inside the chamber
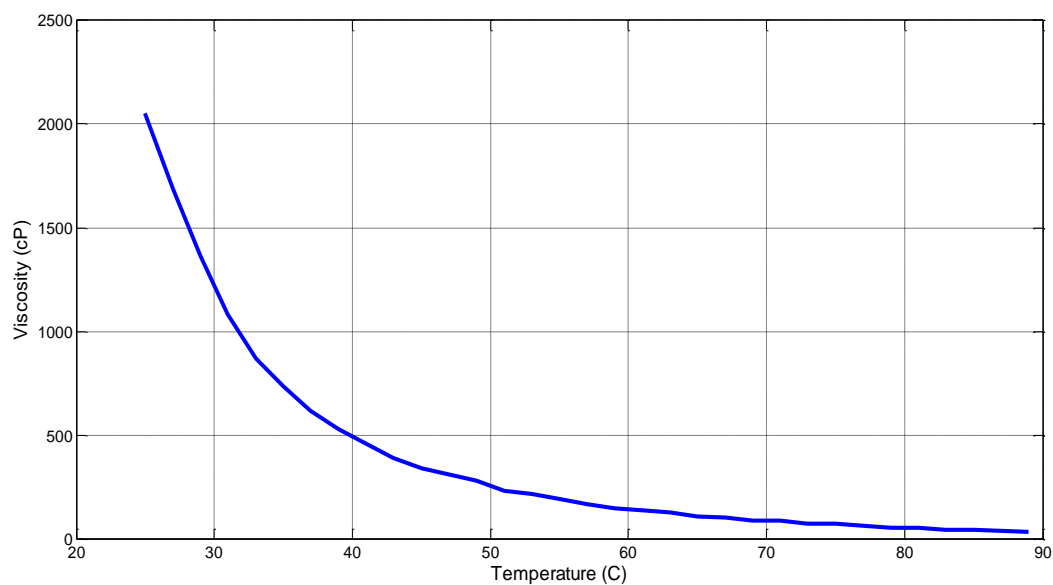


Figure 5 Viscosity vs. temperature of PU 90IK01 one-part resin system
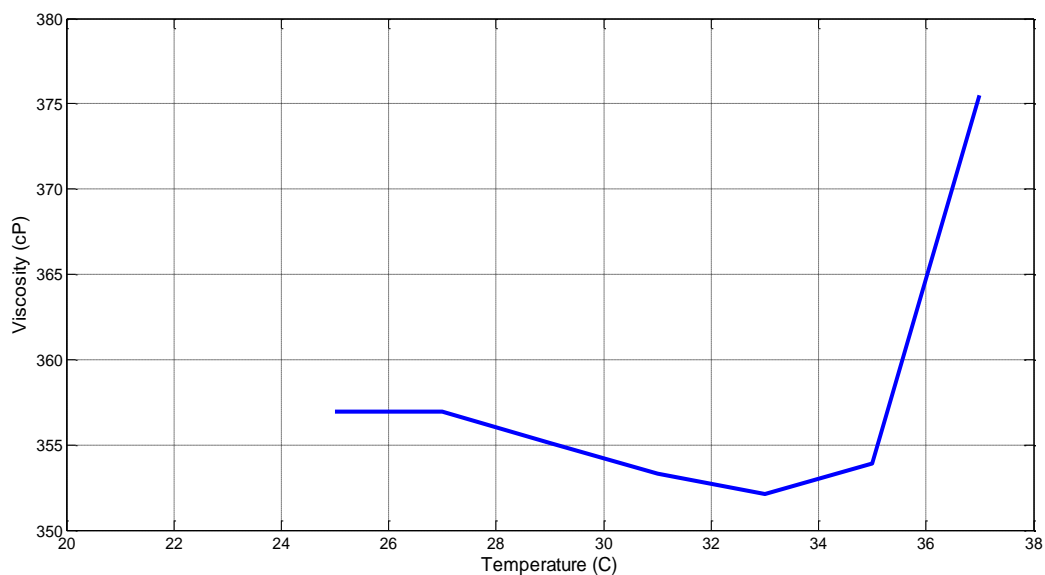
Figure 6 Viscosity vs. temperature of PU 840871 two-part resin system
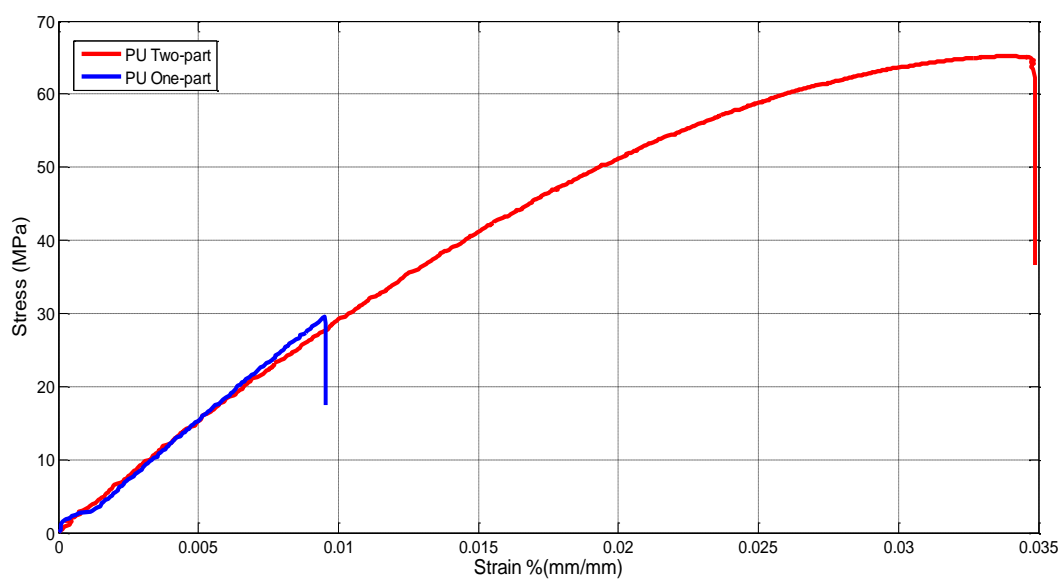


Figure 7 Tensile stress vs. strain of PU 90IK01and PU 840871 neat resins
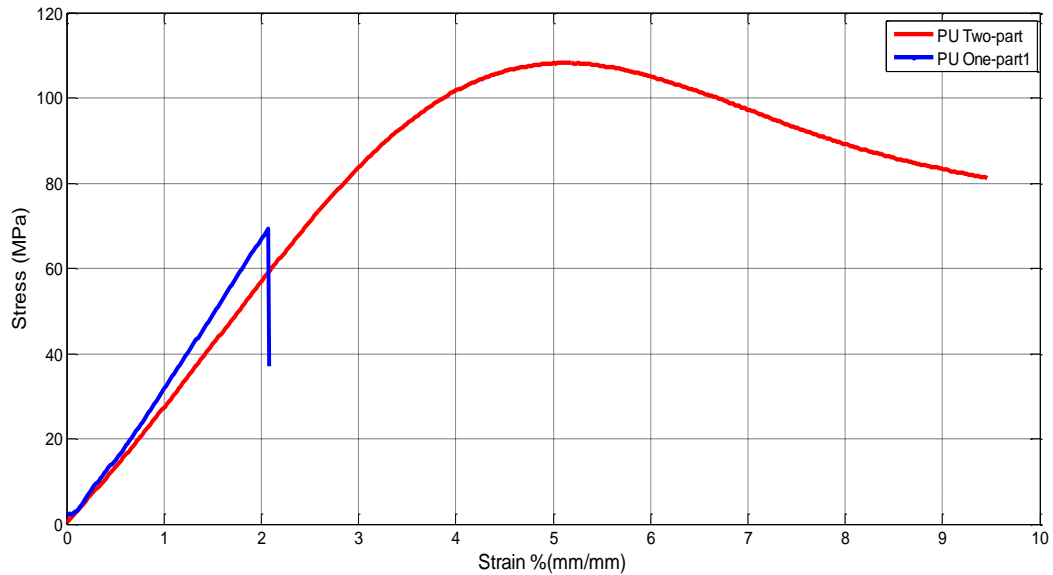
Figure 8 Flexure stress vs. strain of PU 90IK01 and PU 840871 neat resins
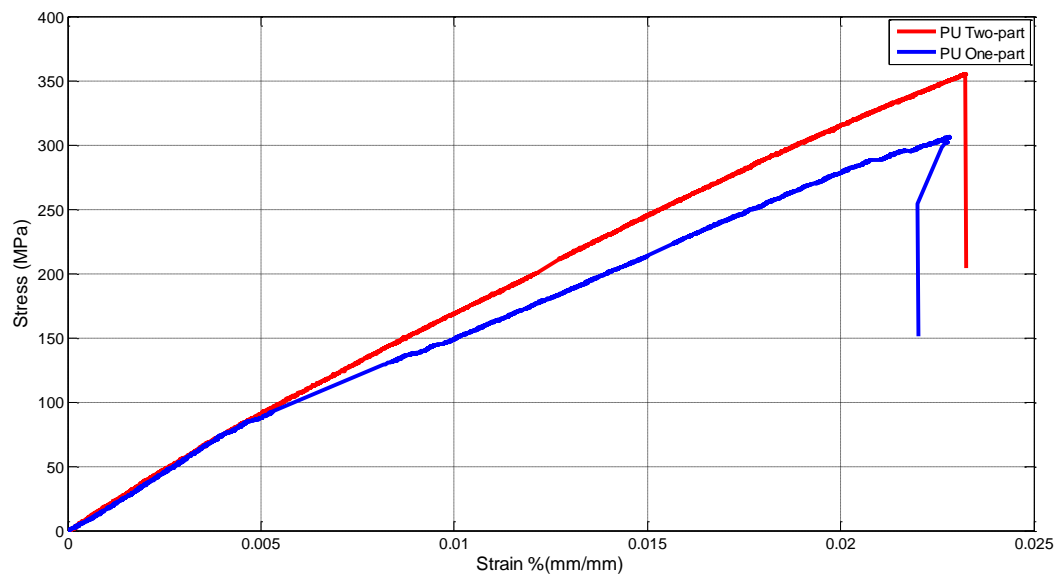


Figure 9 Tensile stress vs. strain of glass fiber/PU 90IK01 and glass fiber /PU 840871
composite laminates

Figure 10 Tensile specimens after testing
The glass fiber/PU840871 specimens (right) typically failed laterally. The glass fiber/
PU90IK01 specimens (left) typically failed by splaying of the fibers.
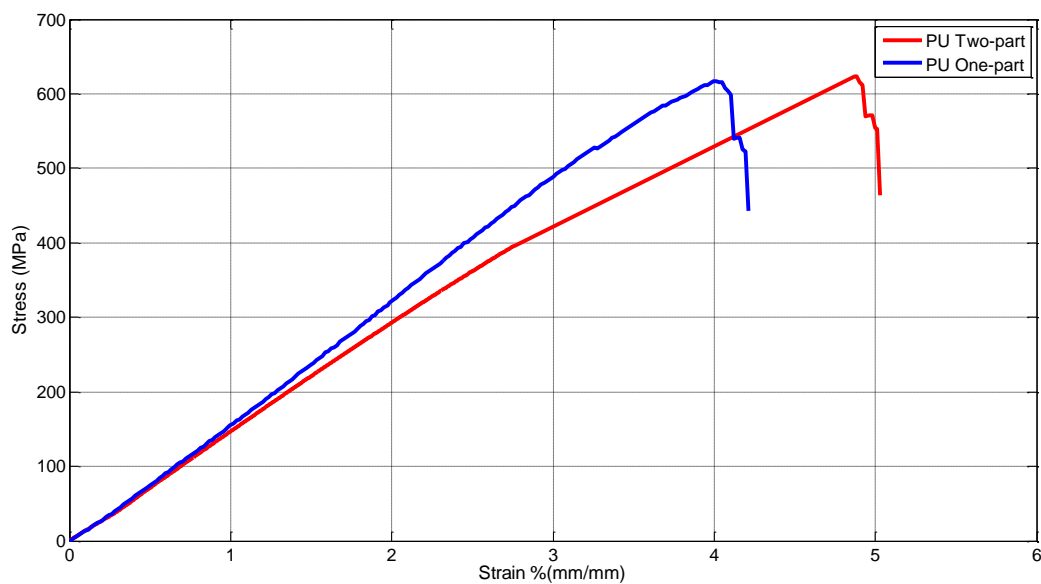
Figure 11 Flexure stress vs. strain of glass fiber /PU 90IK01 and glass fiber /PU 840871 composite laminates
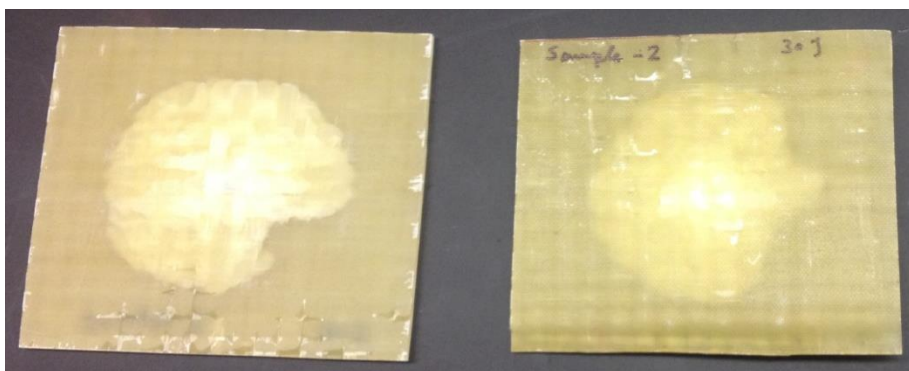


Figure 12 Shows the damaged area of glass fiber/PU90IK01
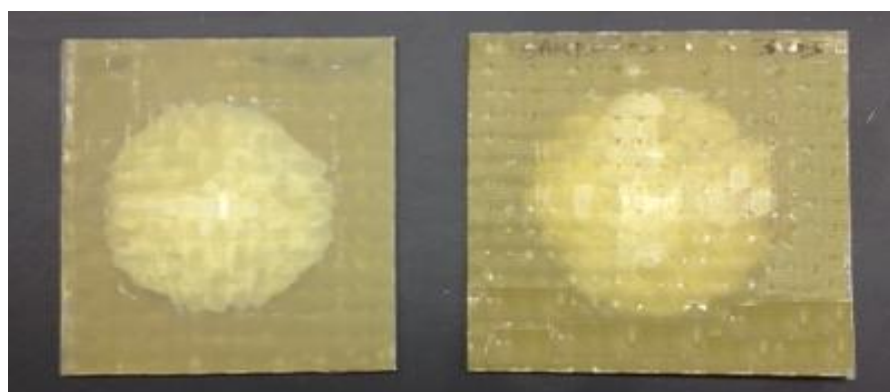


Figure 13 Shows the damaged area of glass fiber/PU 840871
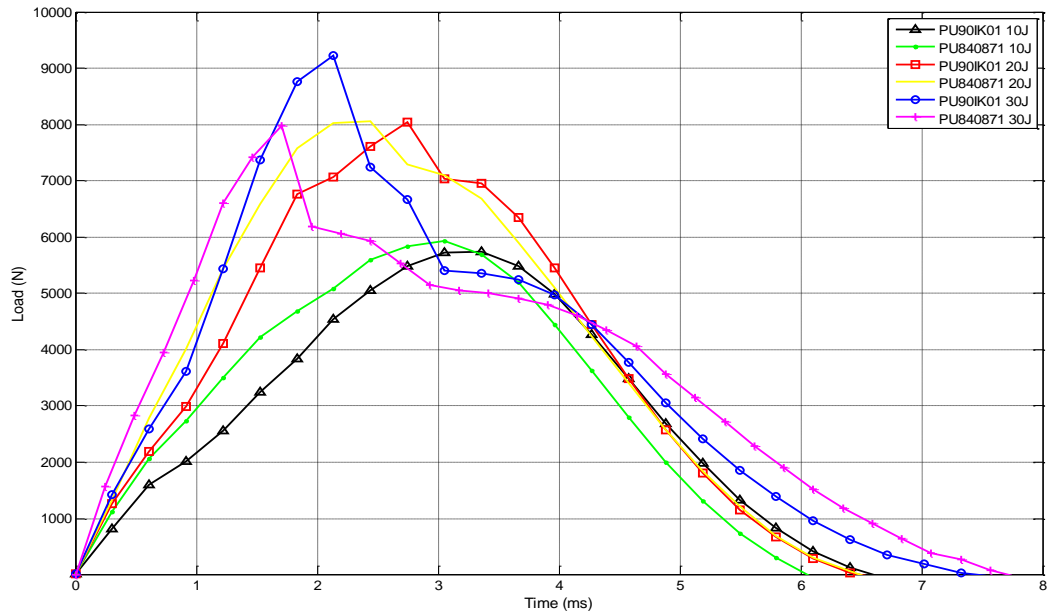
Figure 14 Load vs. time curves recorded in a low-velocity impact test up to failure at different energy levels (10J, 20J, 30J) for glass fiber /PU 90IK01 and glass fiber /PU 840871
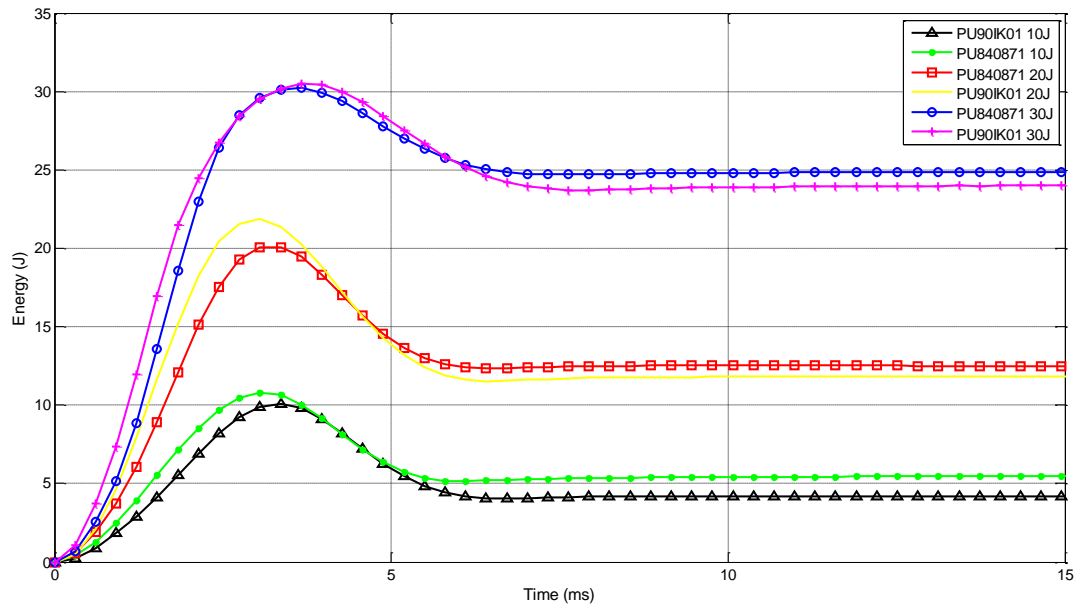


Figure 15 Energy vs. time curves recorded in a low-velocity impact test at different energy levels (10J, 20J, 30J) for glass fiber /PU 90IK01 and glass fiber /PU 840871
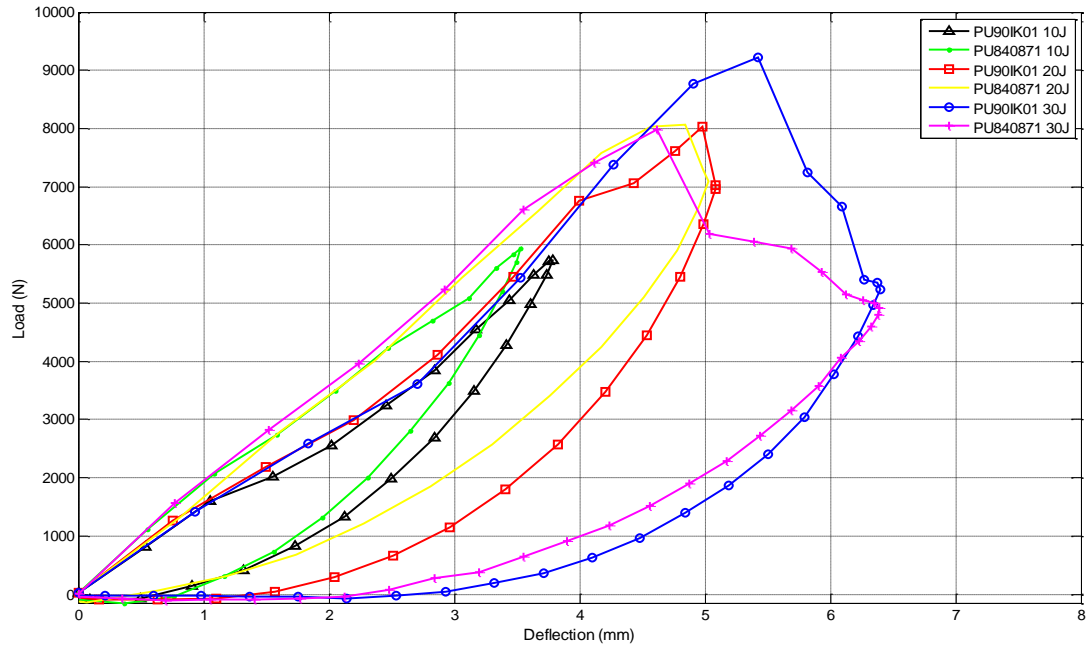
Figure 16 Load vs. deflection curves recorded in a low-velocity impact test up to failure at different energy levels (10J, 20J, 30J) for glass fiber /PU 90IK01 and glass fiber /PU 840871

# II. MANUFACTURING AND CHARACTERIZATION OF POLYURETHANE BASED COMPOSITE BRIDGE DECK PANELS

M. Mohamed[1], S. Anandan[1], Z. Huo[1], V. Birman[1,3], J. Volz[2], and K. Chandrashekhara[1]

[1]*Department of Mechanical and Aerospace Engineering*
[2]*Department of Civil, Architectural and Environmental Engineering*
[3]*Engineering Education Center*
*Missouri University of Science and Technology, Rolla, MO 65409*

## ABSTRACT

Numerous bridges in the USA and worldwide are going through repairing and strengthening operations. Demand has been growing for structural systems utilizing new materials that are more durable and require less maintenance during the service lifetime of the bridge. In particular, composite bridge decks attract attention due to many advantages such as light weight, high strength, corrosion resistance, durability and speedy construction. In this study, three designs of glass reinforced composite deck, namely box, trapezoid and polyurethane rigid foam sandwich types, are fabricated using vacuum assisted resin transfer molding (VARTM) process. The stiffness, load-carrying capacity and compressive strength were evaluated. Flexural, flatwise and edgewise compression tests were carried out for these deck models. The trapezoid model panels under flexural test were modeled and analyzed using commercial finite element method (FEM) software, ABAQUS. The load–time behavior of trapezoid model obtained through simulation was successfully compared with experimental data.

# 1- INTRODUCTION

Composite and sandwich structures are increasingly used in civil infrastructures due to their many advantages such as light weight, high stiffness to weight ratio, corrosion resistance, good fatigue resistance and high durability. The main advantage of a sandwich construction in civil engineering applications is its ability to provide increased flexural strength without a significant increase in weight.

Conventional design of reinforced concrete bridge slabs typically requires a large quantity of steel reinforcement, often causing maintenance problems. Steel reinforcements also increase the weight of the concrete slab. Excessive corrosion in the steel reinforcement caused by de-icing salts and freeze thaw cycles results in inadequate energy absorption under high-impact loads. Using epoxy coated, galvanized or stainless steel bars, concrete surface treatment with siloxanes, and cathodic protection can reduce corrosion but these methods are costly and of limited use. On the contrary, fiber reinforced polymer (FRP) decks ensure that these problems will be avoided to a considerable degree in the future, leading to 50–60 years of service life for FRP bridge decks compared to a typical 15–20 years of service span for concrete bridge decks in North America [1].

With the development of composite manufacturing processes, such as resin transfer molding (RTM), pultrusion and VARTM, modular bridge decks fabricated using polymer matrix composites have been explored since early 1980s. In particular, VARTM is a low-cost composite manufacturing process that has been employed to manufacture various large components including turbine blades, boats, rail cars and bridge decks [2].

Among many applications of composite materials in civil infrastructures, a composite deck for bridges is noteworthy. The composite deck is about 80 percent lighter than a structurally equivalent reinforced concrete deck. Due to quick installation it decreases rehabilitation period so that traffic block time is reduced significantly. Using composite materials to replace concrete deck significantly reduces dead load. Furthermore, in new constructions, lower dead load can translate into savings throughout

the structure, as the size of structural members and foundation is reduced accordingly. The other reason for the use of composite materials is their higher corrosion resistance compared to conventional bridge materials. Accordingly, the service life of a composite deck is much longer than that of a concrete deck due to high durability of composites. In addition, composite decks have strong potential for use in earthquake prone zones and in designs where longer unsupported spans are necessary [3].

Since 1990s, many studies have focused on replacing concrete decks with composite counterparts. A noticeable effort attempting to eliminate such corrosion problem has been conducted by Mufti et al. [4, 5] in developing steel-free concrete deck by using internal bending action in the slab. This concept has been accepted by the Canadian Highway Bridge Code for empirical design methods and has been successfully applied in several field projects in North America. Several concrete deck systems utilizing continuous flat or curved fiber reinforced polymer (FRP) plates have been developed in the recent few years. In 1994, Japanese researchers employed a pultruded glass FRP plate (stiffened with I-beam ribs) that is attached to the bottom of a conventionally designed steel reinforced concrete deck [6]. The 2001 review by Keller [7] looks into the development of some hybrid FRP–concrete systems from 1997 up to 2000. The recent review by GangaRao and Siva [8] evaluates the design and construction details of several all-FRP deck systems that are currently available in North America.

Luke [9] tested a modular E-glass/polyester bridge deck made of several cells 500 mm (19.6 in.) wide, connected using epoxy resin. The cross section of the cell was 225 mm (8.85 in.) deep and had triangular openings with 7.75 mm (0.30 in.) thick webs. It was found that the triangular configuration was not as good as the optimum curved web profile. The deck was approved for 40 ton load as specified by the UK's BS-5400 code.

The Missouri S&T Bridge is an experimental demonstration project that was installed in the fall of 2000 [10]. It represents the first all composite highway-rated bridge in Missouri. It is designed for an AASHTO HS20 highway load rating. The bridge deck is approximately 9.1 m x 2.8 m (358.26 in. x 110.23 in.) and consists of a modular assembly of pultruded 76 mm$^2$ hollow glass and carbon FRP tubes. Carbon/vinyl-ester

tubes are used in the top and bottom layers. Lower-cost, lower-stiffness glass/ vinyl-ester tubes are used elsewhere for economy. Fatigue and failure tests were conducted on 9.1 m x 0.60 m (358.26 in. x 23.6 in.) prototype deck sample, equivalent to a quarter portion of the bridge deck. The FEM results from the model showed good correlation with deflection and longitudinal strains measured during the test.

Hayes et al. (Hayes et al. 2000) [11] tested a 1.22 m (48 in.) wide bridge deck made of glass fibers and polyester matrix. The deck was made up of 12 pultruded square tubes 102 mm x102 mm x 6.36 mm (4 in. x 4 in. x 0.25 in.) sandwiched between two pultruded 9.53 mm (0.37 in.) thick plates resulting in the total depth of (4.76 in.). The elements were connected using epoxy adhesive. Additional lateral tie was provided by through-fiber bolts 25.4 mm (1 in.) in diameter. Shekar et al. [12] reported using E-glass and vinylester resin in construction of four highway bridge decks in the US. The cross-section of the decks was 203 mm (8 in.) deep and used double trapezoidal and hexagonal connectors. The units were assembled at the production plant using polyurethane adhesive. Assembled units were 2.43 m (95.66 in.) in width (in direction of the traffic) and their lengths were equal to the width of the bridge in each case, except for one bridge where the width was covered with two sections linked together longitudinally over the central beam. The decks in four bridges (distance between beams) had varying spans of 762 mm, 889 mm, 1829 mm, and 2591 mm (30 in., 35 in., 72 in. and 99 in.). Aref and Sreenivas [13] conducted field tests and studied the dynamic response of the first FRP composite bridge built in USA. The authors developed a finite element model using MSC-PATRAN and analyzed the structure using ABAQUS.

In this study, three different models of all-fiber reinforced polymer composite sandwich bridge decks utilizing various core designs, namely box, trapezoid and polyurethane (PU) rectangular rigid foam, were fabricated using VARTM process. Woven glass fiber and two part thermoset polyurethane resin systems were used for fabrication. Flexural, flatwise compression and edgewise compression tests were performed accordance to ASTM standards C365, C393 and C364, respectively. In

addition, finite element analysis were conducted using software ABAQUS to model the flexural results for the trapezoid foam model.

## 2- MATERIALS

Three different models were constructed with woven E-glass fiber face sheets. The E-glass fiber, obtained from Owens Corning OH, was compatible with PU resin. A two-part thermoset polyurethane resin system from Bayer Material Science was used as the matrix material. The two-part thermoset resin system (RTM NB #840871) consists of two components. The "A" component is Isocyanate NB#840859 ISO, Diphenylmethane Diisocyanate (MDI-Aromatic). The "B" component is a Polyol (RTM NB#840871), of low viscosity (approx. 350 cPs). The components react rapidly after mixing forming a highly cross-linked thermoset with excellent thermal stability and good mechanical properties.

Three different materials comprised the sandwich's foam core.

- Type-1: high density (6 lb/ft$^3$) PU rigid foam with closed cell (Fig. 1).
- Type-2: low density (2 lb/ft$^3$) polyurethane foam of a trapezoid shape (Prisma) with a combination of two plies and a knitted E-glass biaxial (+/- 45°) matted reinforcement encompassing a single cell (Fig. 2).
- Type-3: web-core boxes with a low density (2 lb/ft$^3$) polyurethane foam and matted reinforcement. It had one additional layer mesh mat of glass fiber between each cell of the core (Fig. 3). The core cells had grooves on their sides to facilitate resin flow across shear webs.

## 3- EXPERIMENTS

### 3.1 Model Composite Decks Fabricated Using VARTM

Most of bridge deck systems are manufactured using pultrusion process. They are connected by chemical bonding and/or mechanical connectors, such as riveting (Huck

bolts) or shear studs, and conventional bolt–nut mechanisms [1]. Three sandwich designs considered in this study are depicted in Fig. 4 that illustrates the model deck sections for the rectangular PU rigid foam, trapezoid shape profile and boxes.

Bridge deck models with E-glass/PU face sheets were manufactured at Missouri S&T composites lab. VARTM, a cost-effective method, was used to fabricate small to large size FRP composite systems. The overall depth was fixed at 54.61 mm (2.15 in.). Each face sheet consisted of three layers of woven E-glass fibers.

Shear layers (E-BXM1715-10) were added during the manufacturing process to the Type 2 model between the trapezoidal sections. The E-glass shear webs increased both the apparent shear modulus of the core as well as the ductility for flexural failure response. The resin was initially cured at room temperature for 6 hours followed by 70 ℃ for 1hr. It was then post-cured at 80 °C for 4 hrs. Figure 5 illustrates the fabrication of specimens using VARTM process. Two panels of dimensions, 914.4 mm x 304.8 mm x 54.61 mm (36 in. x 12 in. x 2.15 in.), were manufactured for each design. The dimensions of test specimens are listed in Table 1.

### 3.2 Flexural Test

Flexural tests of simply supported panels were conducted in accordance with ASTM C-393 (Fig. 6). The length of the support span was equal to 203.2 mm (8 in.). An Instron 5985 test machine with a 250 kN load cell was used to apply load to the sandwich beam specimen at a constant crosshead speed of 6 mm/min (0.25 in/min). Both the location and the type of failure were recorded. Core shear stress at failure, as well as stiffness, were calculated from the resulting load versus deflection curve and the core specimen dimensions.

### 3.3 Flatwise Compression Test

Flatwise tests were performed according to ASTM standard C365M–11. The differences in compressive strengths and elastic moduli of sandwich cores in the direction normal to the plane of the structure between three analyzed designs were investigated.

Tests were performed on an Instron-5985 testing machine with a 250 kN load cell at a rate of 2 mm/min (0.079 in/min). Note that previously, Bitzer [14] found that neither the compressive properties nor the shear moduli vary much as the thickness changes, while the shear strength reduces as the thickness increases. In our experiments, five specimens of each type were tested and the flatwise compression strengths were calculated.

## 3.4 Edgewise Compression Test

The edgewise compressive strength of short sandwich construction samples is important as it provides the basis for the assessment of the load-carrying capacity. Edgewise compression tests of the sandwich bridge deck models were performed on an Instron 5985 machine in accordance with ASTM C364. Compression was applied at a crosshead speed of 10 mm/min using an edgewise compression test fixture (Fig. 7). Sufficiently flat ends were used to prevent localized end failures.

## 4- RESULTS AND DISCUSSION

### 4.1 Flexural Test

### 4.1.1 Comparison of Flexural Strengths

Flexural tests were conducted on the three fabricated deck models (Fig. 8). The failure loads of the deck models, Type-1, Type-2 and Type-3, were 4100 N, 16300 N and 5200 N, respectively. Figure 9 illustrates the load-deflection curve at the center span of the deck model. As expected, the gain in strength in the Type-2 model was quite significant due to the shear layers implanted during the manufacturing between the trapezoid sections.

Type-1 models exhibited maximum deflection because of the foam compaction under loading. Unlike Type-2 and Type-3 models, this model does not have stiffeners that explain its relatively low stiffness. The load–displacement behavior (Fig. 9) was quite similar in the three types of deck models. The experimental data is presented in Table 2 reflecting thatType-2 models carried significantly higher loads than the other models.

Figure 10 depicts the flexural stress-strain curve for the three bridge deck models. The trapezoid shaped foam Type-2 model had a flexural strength four times higher than the other bridge deck models. Due to the E-glass shear webs used in the trapezoid design, both the apparent shear modulus of and the ductility for the flexural failure response increased.

### 4.1.2 Core Shear Stress and Facing Ultimate Stress

In sandwich structures, the core absorbs the shear load while the facesheets carry the bulk of the bending load. Both the core and facesheets was considered for composite sandwich beams tested in this study. Both the core shear stress ($\tau$) and the facesheet bending stress ($\sigma$) values were calculated using the equations given in the ASTM C 393-94. In the following, Equation (1) was used to calculate the maximum core's shear stress ($\tau$) for all types of bending tests. Equation (2) was used to calculate the facing ultimate stress ($\sigma$) for three-point bending test.

$$\tau = \frac{F}{(d+c)b} \tag{1}$$

$$\sigma = \frac{FL}{2(d+c)tb} \tag{2}$$

Where F is the maximum force prior to failure, L is the span length, b is the sandwich width and d, c and t represent the thickness of the sandwich, core and facesheet, respectively.

It is interesting to note that the response of the panel with unreinforced foam core (Type-1) reflects the behavior of closed-cell foams subject to uniaxial compression discussed by Gibson and Ashby [15]. The initial elastic response is followed with a nearly horizontal section of the stress-strain or load-deflection curve. This section corresponds to buckling and crushing of the cell walls. In pure foam specimens such behavior is followed with a densification phase of response as the load increases. In sandwich panels the latter phase is missing due to failure of the entire structure. While the foam response described above is characteristic for uniaxial compression, apparently, the

same features are present in the case of transverse shear loading of the core of a sandwich structure.

### 4.1.3 Effect of Flexural Stiffness ($\phi$)

The facesheet modulus obtained from previous studies for the web-core and PU rectangular models was 19,534.00 MPa [16]. The modulus of the shear layers of the Type-2 model was 14,344.65 MPa. It was obtained from the tensile test performed on the shear layers according to ASTM D3039. The effective flexural moduli of the PU rigid foam, prisma foams and web-core were 8.27 MPa, 4.41 MPa and 4.48 MPa, respectively. These values were obtained from the manufacturing data sheet. As anticipated, the elastic modulus of facesheet is significantly higher compared to the elastic modulus of core.

An important structural property that affects flexural stiffness is the length or loading span. The flexural stiffness is inversely proportional to the length. The modulus of elasticity also influences the flexural stiffness [17]. The functional relationship between the flexural stiffness of the specimen, modulus of elasticity and length is given by Equation (3):

$$\phi \propto \frac{E}{l^3} \tag{3}$$

### 4.2 Flatwise Compression Test

Flatwise compression tests were performed on the bridge deck models to investigate differences in strength and modulus for various core types. Five specimens from each category were tested according to ASTM standard C365M (Table 1). The flatwise compressive strength was calculated using Equation (4) according to ASTM C365M standard:

$$F = {P_{max}}/{A} \tag{4}$$

Where F is the ultimate flatwise compressive strength (MPa), Pmax is the ultimate force prior to failure (N) and A is the area of the surface of facing subjected to compressive load (mm2).

For the average nominal compressive strength and the displacement of Type-1, Type-2, and Type-3 models, respectively, are listed in Table 3. From experimental data, it is determined that for equal core thickness, flatwise compressive strength of Type-2 model is higher than those of Type-1 and Type-3 counterparts due to the strengthening effect of shear layers between the foam cells (Fig.11). The peak compressive load of the Type-2 model was nearly five times higher than that of Type-1 and two times higher than that of Type-3 models.

The first part of the compressive stress–strain curve (Fig. 12) is linear elastic until the stress reaches a maximum for the three models. At this point, the structure begins to fail. In case of Type-1 model, a flat region is observed because of the foam compaction associated with buckling of cell walls described above. In Type-2 and Type-3 models the load drops rapidly due to failure of the stiffening layers. This result is comparable to the observations of Corigliano, et al. [18]. The overall behavior of Type-2 model is governed by the shear layers that behave similar to plates on elastic foundation provided by foam. The postbuckling response of plates being stable, the response is characterized by ascending load-displacement or stress-strain curves until collapse. The response is somewhat different in Type 3 model where both the web is subject to a larger compressive stress under the same load than shear layers in Type-2 model. Although the region of postbuckling web response is detectable, it is much "smaller" and failure occurs at a smaller applied force. It was also noted that adding stitches in the transverse direction to Type-3 model, increases its mechanical performance. The difference between failure of Type-1 and Type-3 models is observed in Fig. 13, 14 where the compaction in the case of Type 1 is evidently different from the failure associated with buckling of web in Type-3 model.

## 4.3 Edgewise Compression Test

Both the compressive properties and the failure behavior of the deck model specimens were analyzed in the course of an in-plane edgewise compressive load. Figure 15 illustrates the deformation and failure of the tested specimens. Specimen failure can take place according to several modes of failure [19]. The overall crushing configurations corresponding to each mode are shown in Fig. 16.

- Mode I: buckling of facesheet

- Mode II: progressive end-crushing of the sandwich facesheet

- Mode III: core compression failure

- Mode IV: core shear failure

The load–displacement curves obtained from the edgewise compression tests conducted on the bridge deck models are depicted in Fig. 17. Experimental results and failure mode identification are listed in Table 4.

The mode I failure (buckling of facesheets) of Type-1 model began at the end of a linear elastic compression phase when the applied load (P) reached a critical value (29,223.51 N). Debonding was observed at the facesheet-to-core interface upon the onset of facesheet buckling. A thin layer of the foam core remained on the debonded facesheet laminates (Fig. 17b) suggesting that debonding could actually be associated with fracture throughout the core propagating close to the interface with the facesheet. This debonding caused a drop in the compressive load followed with the ultimate failure.

In case of Type-2 model, the facesheet initially buckled under compressive load. Buckling was followed with failure of the bond between the foam core and the facing sheet (Fig. 18a). Subsequently, as the buckling zone of the facesheets expanded, extensive cracking and delamination occurred between the layers accompanied by debonding of the core-facesheet interface (Fig. 18b). The shear layer reinforcement resulted in a significant increase in the edgewise compression strength of the panels

reaching 138.55MPa. This is significantly greater than the compressive strength of Type-1 and Type-3 panels (Table 4).

Mode I failure was exhibited by Type-3 models. The thin stiffness layer between the cells of the core resists buckling during the test (Fig. 19). A sudden drop in the compressive load after the initial peak of the force-displacement curve is attributed to failure of the stiffness layer. The critical load, $P_{max}$, for buckling of the facesheet laminates was smaller than that recorded for Type-1 model that failed in mode I.

Facing compressive stress, defined in the ASTM standard C364 as the ratio of the peak load ($P_{max}$) to the loaded face area, is calculated using Equation (5):

$$\sigma = \frac{P_{max}}{[b(2 \times t_f)]} \tag{5}$$

Where $\sigma$ is the ultimate edgewise compressive strength (MPa), $P_{max}$ is the ultimate force prior to failure (N), b is the width of specimen (mm), and tf is the thickness of a single facesheet (mm).

**4.4 Finite Element Analysis**

A three-dimensional explicit dynamic model has been developed to simulate the mechanical behavior of a trapezoid model sandwich structure under three point flexural tests. The modeled sandwich structure consists of three-layer woven E-glass/polyurethane facesheets and trapezoidal low density polyurethane (PU) foam with mat reinforcement represented by three shear layers of E-BXM1715-10 embedded between trapezoidal sections (Fig. 20). To reduce the computational cost, half of overall structure is modeled utilizing symmetry along length direction (Fig. 21). For fiber-reinforced facesheets and reinforcement laminates between foams, a progressive damage model based on continuum damage mechanics [20] is developed using the Hashin failure

criterion to predict damage initiation and evolution. The damage evolution behavior for fiber-reinforced facesheets is reflected in Equation (6):

$$\sigma = \frac{1}{D}\begin{bmatrix} (1-d_f)E_1 & (1-d_f)(1-d_m)v_{21}E_1 & 0 \\ (1-d_f)(1-d_m)v_{12}E_2 & (1-d_m)E_2 & 0 \\ 0 & 0 & (1-d_s)G_{12}D \end{bmatrix}\varepsilon \qquad (6)$$

Where $D = 1 - (1-d_f)(1-d_m)v_{12}v_{21}$, $d_f$ and $d_m$ are the fiber damage index and matrix damage index, respectively, $d_s$ is the shear damage index; $E_1$ is the Young's modulus along fiber direction, $E_2$ is the Young's modulus along matrix direction, $G_{12}$ is the in-plane shear modulus, and $v_{12}$ and $v_{21}$ are Poisson's ratios. Also a crushable foam model is applied for trapezoidal foams. In this crushable foam model, the isotropic hardening yield surface is described by

$$\sqrt{q^2 + \alpha^2 p^2} - \sigma_c\left(\sqrt{1 + (\tfrac{\alpha}{3})^2}\right) = 0 \qquad (7)$$

where pressure stress is $p = -\frac{1}{3}trace\ (\delta)$, the Mises stress $q = \sqrt{\frac{3}{2}(\delta + p\ I)\colon(\delta + p\ I)}$, $\alpha$ is the shape factor of the yield ellipse that defines the relative magnitude of the axes, $\sigma_c$ is the absolute value of the yield stress in uniaxial compression, $\delta$ is Cauchy stress tensor and I is the unit tensor. The facesheet and reinforcement laminates are meshed using 8-node quadrilateral reduced continuum shell elements. The trapezoidal PU foam is meshed using 8-node linear reduced hexahedral elements. The steel loading head and supports were modeled as rigid shells using four-node bilinear elements. Both left and right supports were fully constrained. For steel loading head, all degrees of freedom, except for the displacement along Z direction, were constrained. The rate of loading applied by the steel loading head was 6mm/min (0.236in/min).

Figure 22 illustrates longitudinal stress S11 in the top ply of the reinforcement laminate when the total time elapsed since the beginning of loading equals 45.56 seconds. The maximum tensile stress the longitudinal direction is 242.7 MPa and the maximum

compressive stress is 550.3 MPa. The maximum longitudinal tensile and compressive stresses are located around the corners of the reinforcement laminate, near the loading head. This is predictable because of the stress concentration at these corners. The stress contour along X-axis in the PU foam at the elapsed time equal to 45.56 seconds since the beginning of loading is shown in Fig. 23. Both the maximum compressive stress along the X-axis direction that is equal to 2.18 MPa and the maximum tensile stress equal to 1.84 MPa are located at the corners between the foam and laminate. The function of low density foam is mainly to maintain the shape of sandwich structure but does not contribute much to structural load carrying capability. The maximum tensile and compressive stresses in the longitudinal direction for the first ply of top facing laminate are equal to 368.8 MPa and 218.6.3 MPa, respectively, (not shown here). In the bottommost ply of the bottom facing, the maximum tensile stress in the longitudinal direction is 297.3 MPa, while the maximum compressive stress is 128.3 MPa. These results reflect the load-carrying function of the facings and reinforcing laminate (truss). The punch force-time relationships generated by simulations and experiments are compared are shown in Fig. 24 and found in a reasonable agreement. Up to around 50 seconds, the punch force-time relationship is almost linear, implying that the stress-strain relations for PU foam, facing and reinforcement laminates remain in the elastic range. Eventually, the foam experiences collapse/densification, while the facings and reinforcement laminates undergo progressive damage initiation and evolution resulting in a nonlinear response until the ultimate failure.

## 5- CONCLUSION

Glass fiber/polyurethane composite decks with three types of foam cores, namely rigid PU foam, prisma foam, and web-core, were successfully manufactured using VARTM process. Performance evaluation of E-glass fiber/PU sandwich composites models was conducted using flexure, flatwise compression, and edgewise compression tests to determine the respective stiffness and strength of the models.

Flexural testing of the manufactured sandwich panels proved that Type-2 models have the highest load carrying capacity in bending. In addition, Type-2 model carried the maximum load under flatwise and edgewise compression due to the presence of shear layers. A finite element model was developed using ABAQUS, for Type-2 model. The three point dynamic bending behavior was found to be in agreement with the experimental results. Based on the experimental and numerical results, it is suggested that sandwich panels with prisma cores represent a preferable design for bridge decks. Future work will include the construction of a full scale composite bridge using the prisma core as well as experimental verification of the stresses in the facings and reinforcing laminates (truss).

## 6- ACKNOWLEDGEMENT

# 7- REFERENCES

[1] Dong, C., "A Modified Rule of Mixture for the Vacuum-Assisted Resin Transfer Molding Process Simulation," *Composites Science and Technology, Vol.*68, pp. 2125–2133, 2008.

[2] Scott, R.R., "FRP Composite Bridge Deck Barriers to Market Development," *National Composite* Center, Ohio, 2000.

[3] Alagusundaramoorthy, P. and Reddy, R.V.S., "Testing and Evaluation of GFRP Composite Deck Panels," Ocean Engineering, Vol. 35, pp. 287-293, 2008.

[4] Bakht, B. and Mufti, A.A., "Five Steel-Free Bridge Deck Slabs in Canada," Structural Engineering International, Vol. 8, pp. 196–200, 1998.

[5] Edalatmanesh, R. and Newhook, J.P., "Investigation of Fatigue Damage in Steel-free Bridge Decks with Application to Structural Monitoring," ACI Structural Journal, Vol.110, pp. 557-564, 2013.

[6] Jain, R. and Lee, L., "Fiber Reinforced Polymer (FRP) Composites for Infrastructure Applications," Technology Reports of the Osaka University, Vol.44, pp. 295-307, 1994.

[7] Keller, T, "Recent All-composite and Hybrid Fibre-Reinforced Polymer Bridges and Buildings," Progress in Structural Engineering and Materials, Vol. 3, pp. 132–140, 2001.

[8] GangaRao, V.S. and Siva, R.V., "Advances in Fibre-Reinforced Polymer Composite Bridge Decks," Progress in Structural Engineering and Materials, Vol 4, pp. 161-168, 2002.

[9] Luke, S., "The design, installation, and monitoring of an FRP bridge at West Mill, Oxford," Lightweight Bridge Decks: European Bridge Engineering Conference, Rotterdam, the Netherlands, pp. 1-12, (2003.

[10] Kumar, P., Chandrashekhara, K. and Nanni, A., "Structural Performance of a FRP Bridge Deck," Construction and building Materials, Vol. 18, pp. 35-47, 2004.

[11] Hayes, M.D., Lesko, J.J., Haramis, J., Cousins, T.E., Gomez, J. and Massarelli, P., "Laboratory and Field Testing of Composite Bridge Superstructure," Journal of Composites for Construction, Vol 4, pp. 120-128, 2000.

[12] Shekar, V., Petro, S.H. and GangaRao, H.V.S., "Fiber-Reinforced Polymer Composite Bridges in West Virginia," Transportation Research Board , Vol. 2, pp. 378-384, 2003.

[13] Aref, A.J. and Alampalli, S. "Vibration Characteristics of a Fiber-reinforced Polymer Bridge Superstructure," Design and Manufacturing of Composite Structures , Vol 52, pp. 467–474, 2001.

[14] Bitzer, T. "Honeycomb Technology," Chapman and Hall, California, pp.98-116, 1997.

[15] Gibson, L.J. and Ashby, M.F., "Cellular Solids: Structure and Properties," Cambridge University Press, Cambridge, 1997.

[16] Mohamed, M., Vuppalapati, R.R., Hawkins, S., Chandrashekhara, K. and Schuman, T., "Impact Characterization of Polyurethane Composites Manufactured using Vacuum Assisted Resin Transfer Molding," International Mechanical Engineering Congress & Exposition, Houston, Texas IMECE2012-88267, pp. 1-8, 2012.

[17] Santhanakrishnan, R., Dash, P.K., Joseph, S.A. and Sabarish, M. "Flexural Property Evaluation of GFRP-foam Sandwich Composite - An Experimental Approach," ARPN Journal of Engineering and Applied Sciences , Vol. 7, pp. 1300-1306 2012.

[18] Corigliano, A., Rizzi, E. and Papa, E., "Experimental Characterization and Numerical Simulations of a Syntactic-foam/Glass-fiber Composite Sandwich," Composite Science and Technology , Vol. 60, pp. 2169-2180, 2000.

[19] ASTM C364/C364M–07 Standard Test Method for Edgewise Compressive Strength of Sandwich Constructions.

[20] ABAQUS Theory Manual, Version 6.10. Pawtucket, RI: Hibbitt, Karlsson and Sorensen, 2010.

Table 1 Test specimen specifications

| Test | Specimen Model type | Facesheet Constituents | Dimensions | | |
|---|---|---|---|---|---|
| | | | Length (in.) | Width (in.) | Thickness (in.) |
| Flexure | Type-1 | E-glass/PU | 10 | 2.95 | 2.15 |
| | Type-2 | E-glass/PU | 10 | 2.95 | 2.15 |
| | Type-3 | E-glass/PU | 10 | 2.95 | 2.15 |
| Flatwise Compression | Type-1 | E-glass/PU | 1.75 | 2 | 2.15 |
| | Type-2 | E-glass/PU | 1. 75 | 2.15 | 2.15 |
| | Type-3 | E-glass/PU | 1.75 | 2 | 2.15 |
| Edgewise Compression | Type-1 | E-glass/PU | 8 | 4 | 2.15 |
| | Type-2 | E-glass/PU | 8 | 4 | 2.15 |
| | Type-3 | E-glass/PU | 8 | 4 | 2.15 |

Table 2 Flexural test results

| Specimen Model Type | Flexural Strength (MPa) | Flexural Failure Strain (%) | Maximum Load (N) | Facing Ultimate Stress (MPa) | Core Shear Stress (MPa) |
|---|---|---|---|---|---|
| Type-1 | 6.10 ±0.4 | 0.19 ±0.02 | 4477.91 ±112 | 22.84 ±1.2 | 0.57 ±0.2 |
| Type-2 | 21.52 ±1.1 | 0.16± 0.04 | 16371.16 ±110 | 41.78 ±1.6 | 2.02 ±0.6 |
| Type-3 | 6.41 ±0.8 | 0.07 ±0.01 | 4708.26 ±89 | 27.67 ±1.4 | 0.60 ±0.1 |

Table 3 Flatwise test results

| Specimen Model Type | Maximum Load (N) | Ultimate Flatwise Compressive Stress (MPa) | Failure Compressive Strain (%) | Deflections (mm) |
|---|---|---|---|---|
| Type-1 | 2357.54 ± 131 | 1.21 ± 0.1 | 0.38 ± 0.05 | 21.29 ± 3 |
| Type-2 | 9230.53 ± 157 | 3.81 ± 0.2 | 0.09 ± 0.02 | 6.03 ± 0.8 |
| Type-3 | 5477.19 ± 95 | 2.82 ± 0.2 | 0.22 ± 0.01 | 12.02 ± 2 |

Table 4 Edgewise compression test results

| Specimen Model Type | Maximum Load (N) | Ultimate Edgewise Compressive Stress (MPa) | Deflection (mm) | Failure Mode |
|---|---|---|---|---|
| Type-1 | 28032.51 ± 126 | 76.40 ± 2.3 | 6.49 | I |
| Type-2 | 102050.34 ± 171 | 138.55 ± 1.4 | 10.26 | I,II |
| Type-3 | 20670.24 ± 104 | 62.37 ± 2.1 | 3.01 | I |

Figure 1 Type-1 high density PU foam



Figure 2 Type-2 Trapezoidal low density foam with mat reinforcement



Figure 3 Type-3 Web-core foam with mat reinforcement



Type-1                          Type-2                          Type-3
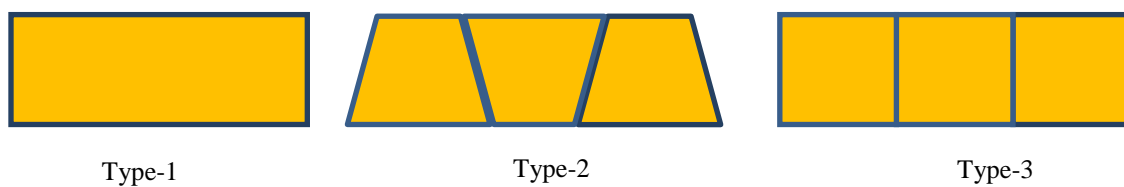
Figure 4 Bridge deck models

Figure 5 VARTM setup for sandwich composite
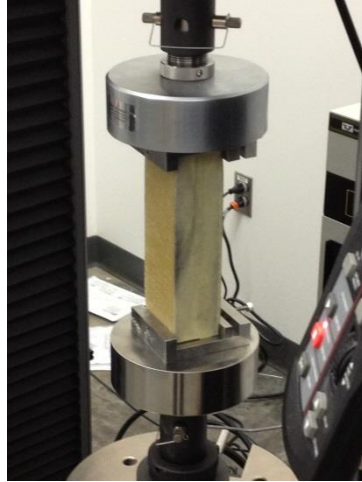


Figure 6 Flexural test setup

Figure 7 Edgewise test setup


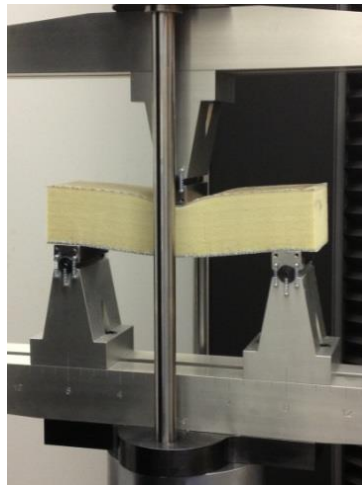
Figure 8 PU rigid foam Type-1 during the test
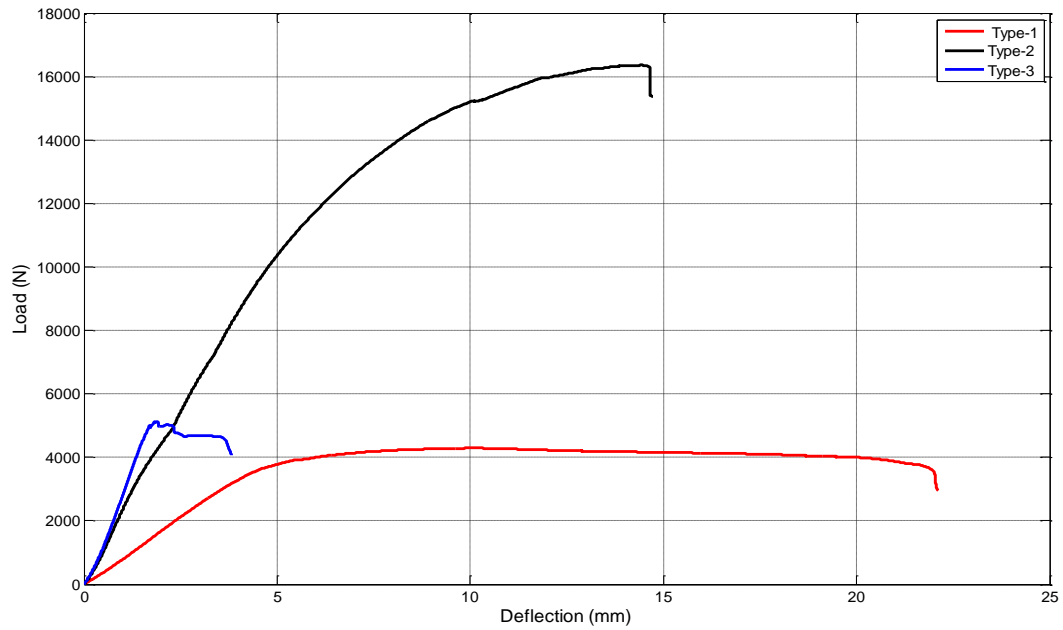
Figure 9 Load vs. deflection curve generated in the flexural test
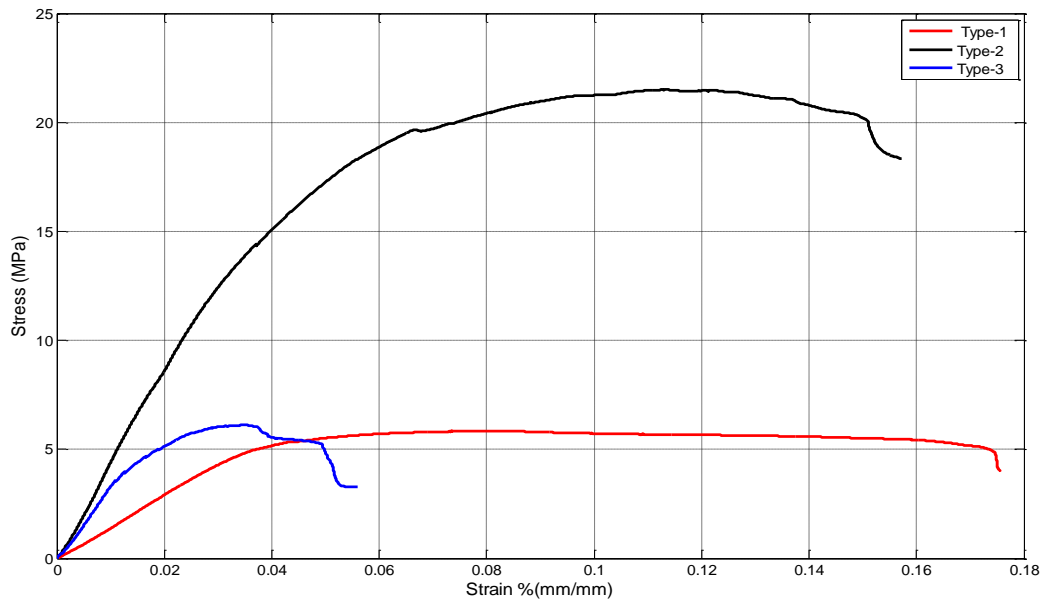


Figure 10 Stress vs. strain curve generated in the flexural test
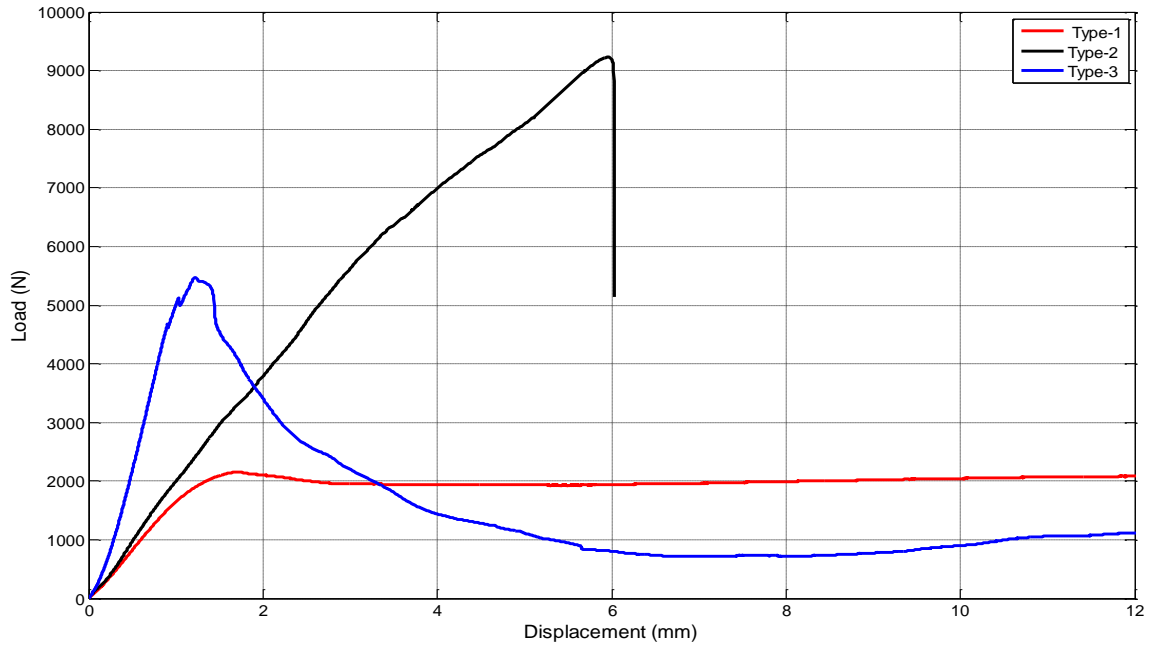
Figure 11 Load vs. Deflection curve in flatwise compression test
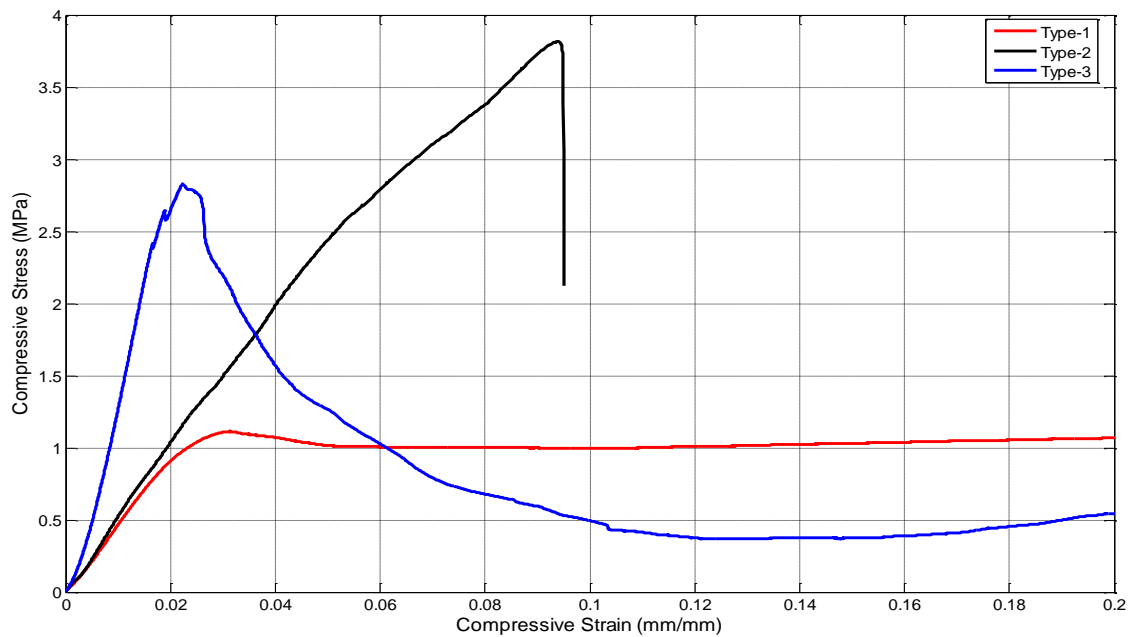


Figure 12 Stress vs. Strain curve in flatwise compression test

Figure 13 Samples Type-1 during testing



Figure 14 Samples Type-3 during testing

Facesheet
buckling failure

Facesheet
compression failure

Core
compression
failure

Core shear
failure
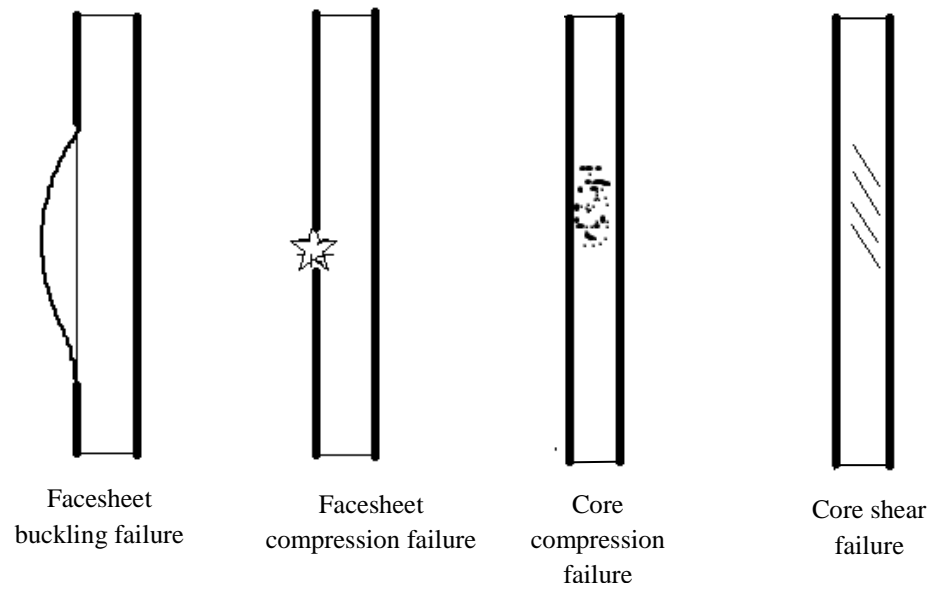
Figure 15 Failure modes of sandwich structures
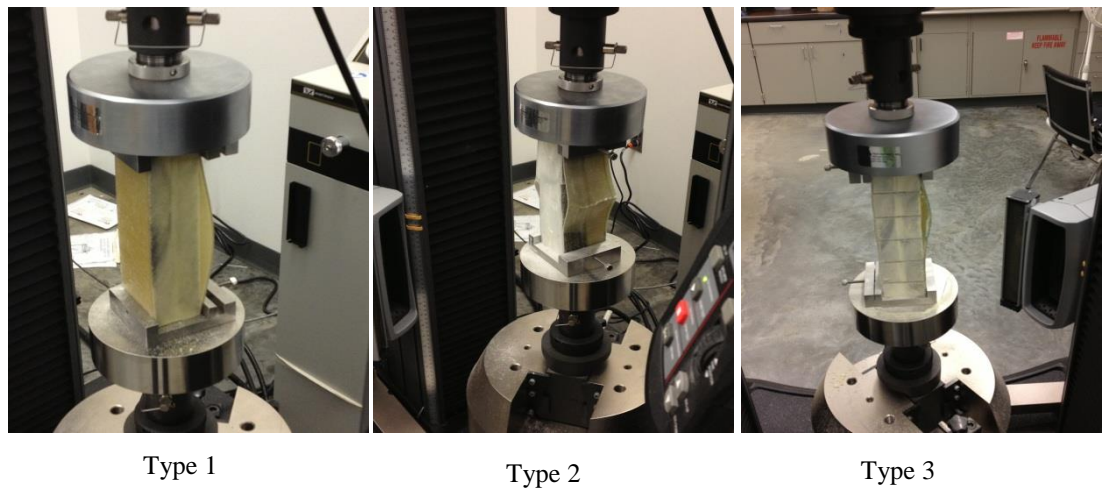
Type 1

Type 2

Type 3

Figure 16 Crushing configurations of the three models
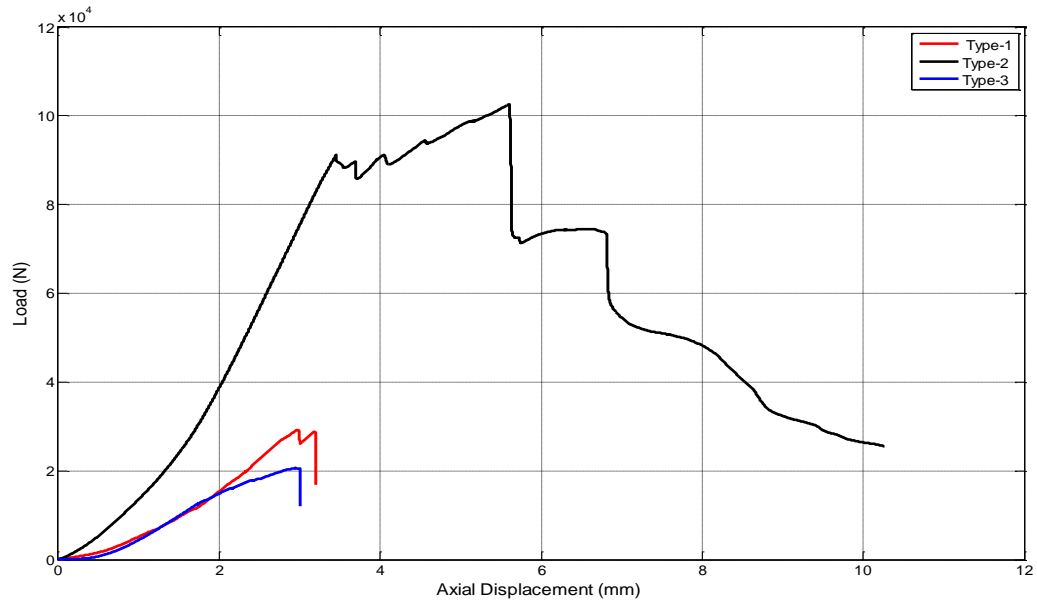
Figure 17 Load–displacement curves from the edgewise compression test
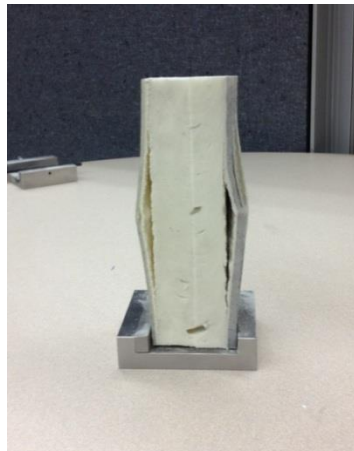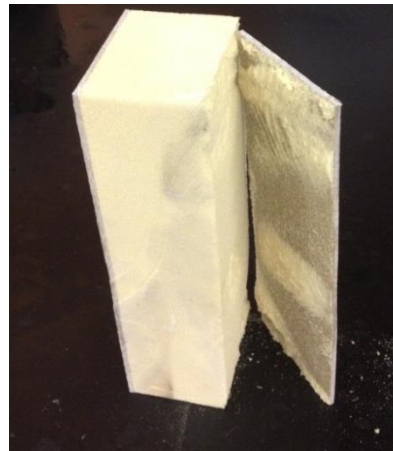


a                                        b

Figure 18 a: Failure of Type-2 model      b: Facesheet debonding of Type-1 model

Before the failure                After the failure

Figure 19 Type-3 model before and after failure
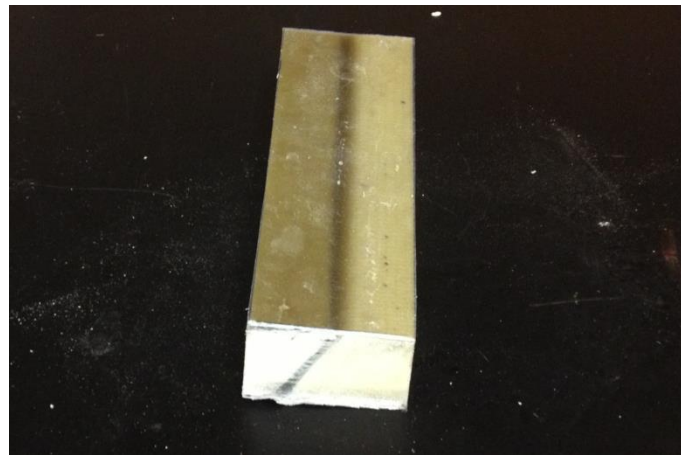


Figure 20 Geometry of sandwich panel with trapezoidal foam sections (Type 2 model)
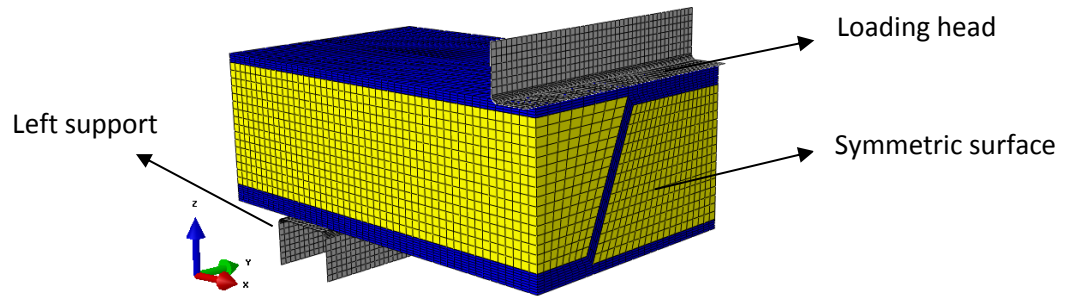
Figure 21 Half modeling mesh of sandwich panel with trapezoidal foam sections
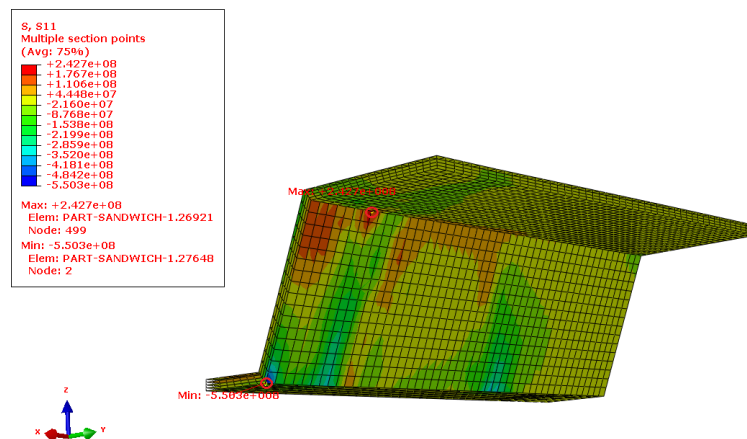


Figure 22  Longitudinal stress S11 in the top ply of the reinforcement laminate when t=45.56 seconds
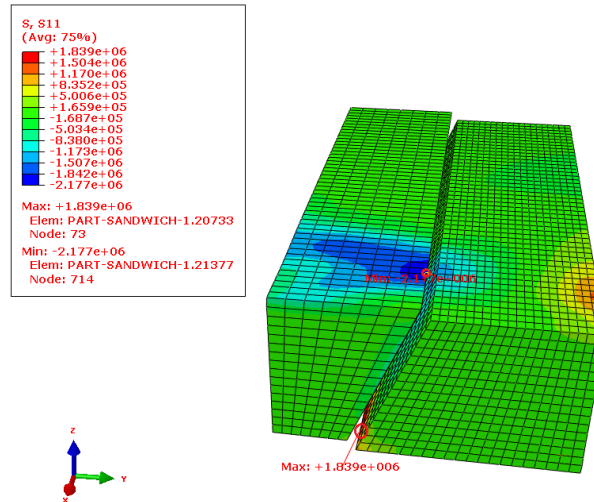
Figure 23 Stress contour along the X-axis for PU foam when t=45.56 seconds
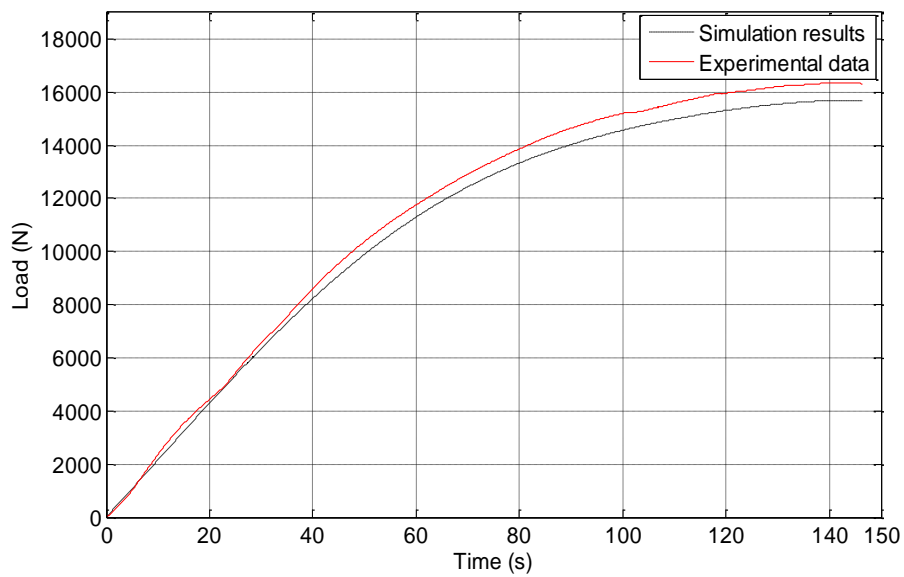


Figure 24 Comparison between simulation results and experimental findings in term of punch force vs. time

# III. PERFORMANCE EVALUATION OF POLYURETHANE COMPOSITE STRUCTURAL INSULATED PANELS (CSIP) FOR MODULAR HOUSE

M. Mohamed[1], R. Hussein[1], A. Abutunis[1], Z. Huo[1] and K. Chandrashekhara[1,]
L. H. Sneed[2]
[1]*Department of Mechanical and Aerospace Engineering*
[2]*Civil, Architectural and Environmental Engineering*
*Missouri University of Science and Technology, Rolla, MO 65409*

## ABSTRACT

Composite materials are now being extensively employed in new applications of civil and building materials. The new generations of two-part thermoset polyurethane (PU) resin systems are desirable materials for infrastructure applications. This is due to good impact resistance, superior mechanical properties and reduced volatile organic compounds when compared to the conventionally used resin systems such as vinyl ester, polyester and vinyl alcohol. Glass fiber reinforced two-part PU composites and low density polyurethane foam are used to design and manufacture composite structure insulation panels (CSIP's) using vacuum assisted resin transfer molding (VARTM) process for temporary housing applications. Using these types of composite panels in building construction will result in cost efficient high performance products due to inherent advantages in design flexibility. Use of core-filled composite structures offers additional benefits such as high strength, stiffness, lower structural weight, ease of installation and structure replacement, and higher buckling resistance than the conventional panels. Energy efficiency is known to be inherently better with the core-filled composite panel than in a metallic material. The panels can be designed to take the required loads and for large panels, stiffeners can be integrated while manufacturing and will play the role of joist/studs. The study aids to evaluate the ability of lab scale tests and models to predict part quality in full-scale parts. Furthermore, it discusses the manufacturing challenges. Flexure tests and energy consumption evaluations were performed on these structural components. Numerical simulation results were used to validate the flexural experiment findings.

# 1- INTRODUCTION

Polymer composite materials have found applications in automotive, aerospace and infrastructure. Compared to most metals, non-metals and unreinforced plastics, they offer a high strength-to-weight ratio, corrosion resistant, are non-conducting, durable and can be fabricated into complex shapes. Composite materials are also being used in the repair and construction of civil infrastructure systems; there has been a great push to develop markets for composites in the building industry. However, high material and fabrication costs virtual to traditional construction materials (steel, concrete and wood) have limited the use of polymer composites to very specific applications that take advantage of unique properties of the composite materials. In recent years, fiber reinforced polymer (FRP) composites have been increasingly used in highway bridge decks [1]. Fiber reinforced composites are also being used to repair or strengthen reinforced concrete bridges and other structures [2]. Some of the more successful applications include seismic retrofitting of reinforced concrete bridge columns using FRP wraps, strengthening of reinforced concrete slabs and girders with FRP plates and tow sheets, FRP bridge decks, and in the design of marine and coastal structures where composites are immune to corrosion and degradation by marine organisms [3].

Recently, Structural Insulated Panels (SIPs), a type of sandwich panel made from oriented strand board (OSB) facesheet and foam are already in use in residential construction in the U.S. Composite sandwich panels fabricated using FRP skins and a lightweight foam core material, such as polyurethane, have been proposed for housing applications, due to their high insulation properties. Their light weight also means that larger housing components can be fabricated in the plant and easily to transported and assembled in the field, with fewer connections. The structural design and materials used in housing construction can be improved through the development and application of composite materials that capitalize on multifunctional components. This can be achieved

by using panelized construction. Panelized systems developed and analyzed in this paper are based on the theory of sandwich structures.

Today, structural insulated panels with OSB skins have penetrated the single and multifamily residential and light commercial construction market as exterior wall components. Composite structural insulation panels (CSIP) proposed in present work to reduce maintenance, construction time, labor intensity and provide cost saving for its inhabitants. The reduction of thermal bridging, air infiltration, and increase in thermal resistance, when comparing CSIP construction with typical SIP construction, demonstrates a great reduction in building energy consumption as the results show in this study. This reduction is so great that CSIP's construction is now being targeted as a net zero energy option when used with other energy saving strategies and mechanisms. L. Smakosz and J.Tejchman [4] experimentally investigated the strength, deformability and failure mode of composite structural insulated panels with expanded polystyrene foam (ESP). the experimental results showed that the CSIP's overcome deficiencies of traditional SIP's. T. Sharaf, et al. [5] studied the flexural behavior in three-point and four-point bending of a new sandwich panel with two different core densities proposed for cladding buildings. The results showed that flexural strength and stiffness increased substantially, by 165% and 113%, respectively, as the core density was doubled. The contributions of shear deformation of the soft and hard cores to mid-span deflection were 75% and 50%, respectively. Rama. R. Vuppalapati et al. [6] Manufactured and tested core-filled pultruded composite panel using novel pultrusion set-up and bio-based polyester and polyester resin systems. The manufactured composite panels were tested for their mechanical properties through tensile, flexure and different impact energy levels. The results indicate that the core-filled panel's soy-based composite panel's exhibit improved impact resistance as compared to the base polyester panels. A. Bezazi, et al. [7] examined the behavior of sandwich panels fabricated from materials with different properties under static loading in three-point bending. The study compared the behavior of the sandwich panel to those of the individual constituents under the same loading conditions. The results showed that in terms in stiffness and load at failure the

effects of core density and its thickness on the behavior and the damage was significant, and the sandwich structure has better mechanical characteristics compared to its components.

House panel insulation efficiency is a main part of reducing energy needed for space heating and cooling. In the United State, every year buildings are accountable for almost half of the total energy consumption and the associated $CO_2$ emissions. According to the U.S Department of Energy (DOE), 2012, U.S is responsible for 19% of the total world primary energy consumption in the transportation, commercial, residential and industrial sectors. The building sector accounted for about 41% of the U.S primary energy consumption and the other 60% attributed, almost evenly, to the industrial and the transportation sectors. This growth in buildings sector energy consumption is fueled primarily by the growth in population, households, and commercial floor-space, which are expected to increase 27%, 31%, and 28%,  respectively, between 2009 and 2035 [8].

Detailed research has been conducted regarding energy consumption of SIPs. Kawasaki and Kawai [9] studied the thermal properties of various wall construction techniques and found that SIP walls perform better than traditional stud walls due to their increased density and thickness. However, additional research that quantifies the effects of these design options in combination is needed to provide meaningful results. Hastings [10] reports from the outcome of four multiphase building projects where the house lacks a conventional heating system because of high insulation levels and low energy requirements for heating. One of the conclusions is that load management, such as setting the thermostat lower at night, saves little energy due to the time constant (presupposing that the windows are closed).

Another review of low-energy buildings around the world is presented where thick insulation, air-tight construction, ventilation with heat recovery and high performance windows are common technologies to decrease the energy demand. Christian, J. et al. [11] described the thermal performance of the third in a series of five affordable, near zero-energy house prototypes built in Lenoir City, Tennessee. Key finding is that the PV could be expanded to attain zero energy status. The net cost per day

for all off-site energy also has been progressing downward. Hester, N et al. [12] developed a model and analyzed the effectiveness of a range of energy-saving measures for residential houses in semi-arid climates. These energy-saving measures include: structural insulated panels for exterior wall construction. This modeling effort compares the energy-use of various building designs in a particular climate. The result shows that, energy consumption is reduced by up to 6.1% when multiple energy savings technologies are combined.

## 2- OBJECTIVE

In traditional construction, different layers of materials and structural components are brought separately and assembled, with each typically sustaining a single primary function. For example, insulation is placed in the wall to provide energy efficiency. Gypsum wallboard is placed to provide a finished surface; a stud wall consists of studs to provide structural resistance to gravity. These separate components are required to provide separate functions. These components can be replaced by one sandwich panel, referred as CSIP, which is durable and can perform all of these functions and provide much higher strength. CSIP can be manufactured in one place and is easy to transport due to its light weight. Although the materials used in this work are cheap and low prices in comparison to the traditional used materials in construction building. For example, E-glass reinforced FRP are much cheaper than steel. FRPs are also characterized by high corrosion resistance as well as high durability, which reduce future maintenance and overall life cycle costs. In addition, the quantity of FRPs used for manufacturing the panels is very low in which one laminate (facesheet) of thickness 3mm (.012in.) can carry much higher loads than traditional construction. Moreover, the processing method of the panels proposed in this study saves manufacturing time and does not require any skilled labors, thus reducing the cost. As a result of savings in time, materials, and labor, potential exists for significant cost reduction compared to the traditional construction.

The main objectives for this work were to compare two systems for wall panels, the first one by using oriented strand board (OSB) and core material (BASF Autofroth 2-

part Foam: 9300A Isocyanate) manufactured by Thermocore of Missouri, LLC and the second CSIP by using thermoset polyurethane resin systems as matrix, bidirectional E-glass fiber as reinforcement materials and 2.00 lb density polyurethane foam core manufactured with VARTM at Missouri S&T composite lab. To assess a small-scale E-glass/PU panel's performance under a four-point bending test, energy efficient and discuss results in terms of load, deflection and energy savings. It is anticipated that the experimental and analytical results presented would be a first step towards the long term goal of manufacturing full-scale composite wall panel for building construction and providing a practical method to predict deflections, stress, and ultimate load.

## 3- MATERIALS AND MANUFACTURING

### 3.1 Facesheet and Core Material

Figure 1 presents the cross-section of a single CSIP. The facings, made from a bi-directional E-glass fabric which is compatible with PU resins are obtained from Owen Corning, OH was used as reinforcing material. Woven fiber based composites offer improved performance over unidirectional type composites. New generation two-part thermoset polyurethane (PU) resin system from Bayer MaterialScience was used as the matrix material. The two-part PU resin comes in two separate parts which will react once combined. The "A" component is an Isocyanate NB#840859 ISO, Diphenylmethane diisocyanate (MDI- Aromatic) and the "B" component is a Polyol RTM NB#840871. The mix ratio by weight for the A and B components is 92:100. These two components are referred to as a PU 840871 resin system of low viscosity (approx. 350 cPs). The components react rapidly after mixing forming a highly cross-linked thermoset with excellent thermal stability and good mechanical properties. The core of the analyzed CSIP is made from polyurethane (PU), the light-weight, soft low density $(38kg/m^3)2.00$ $lb/ft^3$ and closed-cell foam with thickness 118mm (4.65in.) commonly used as a thermal insulation building material was provided by ITW insulation system, TX.

### 3.2 Manufacturing Process

Composite structural insulation sandwich panels 1220 mm x 203 mm x 120.6 mm (48in. x 8in x 4.75in.) were manufactured at Missouri University of Science and Technology (Missouri S&T) composite lab using a cost-effective method VARTM process. The cost of manufacturing process of composite parts usually represents a major portion of the total cost. For use in housing, the fabrication of panels or whole house systems must be simple and inexpensive for them to be competitive with traditional construction materials. This excludes some methods for composite manufacturing, such as injection molding. Most of sandwich panel systems are manufactured using pultrusion process. Currently the most viable fabrication method for very large composite parts is VARTM. Vacuum assisted resin transfer molding uses atmospheric pressures and involves low-energy consumption to cure the composite. Manufacture VARTM process uses a rigid mold on one side and flexible mold (bagging material) on the other side. Fiber reinforcement lay-up is arranged on the rigid mold and the mold is closed using the flexible bagging material. Resin inlet is placed on one corner and vacuum outlet is placed on the other corner. Release film is applied on the mold prior to the placement of fiber lay-up to enable easy removal of the cured part and avoid resin sticking to the mold. Peel-ply is used on either side of fiber lay-up to avoid part sticking to vacuum bag and the mold. High permeability layers were used on either side to the E-glass fibers to reduce the resin infusion time. The mold is closed by applying tacky tape on all sides. The infusion of PU resin was conducted at room temperature and takes approximately 10 minutes to complete the process. Once all the fibers are wet, excess resin escapes through the vacuum outlet into a pre-arranged resin trap. The resin was cured at 70 ºC for 1hr. then post-cured at 80 °C for 4 hrs. in a walk-in oven Fig. 2 illustrates the fabrication of specimens using VARTM process. Eight panels were manufactured, the external facesheet used in CSIPs considered in the paper were 3mm (0.12in.) thick and reinforced with three layers of woven glass–fiber. The fiber volume fraction for the glass-reinforced PU composites fabricated by VARTM is 56%.

PU resin system is moisture sensitive. To address this issue, the mold and all materials were heated to 200°C and cooled to the room temperature to ensuring removal of all moisture from the mold. This process is done prior to placement of fabric lay-up. Also, PU resin was degassed before vacuum infusion such that any entrapped air bubbles are removed, which results in a high quality part. At the end of the manufacturing process, the final thickness of the CSIP was measured to be approximately 203mm (4.75in.)

## 4- EXPERIMENT TESTING AND RESULTS DISCUSSION

### 4.1 Flexure Test

To characterize the structural response of the composite structural insulation panels, the specimens were subjected to a four-point bending test. The flexural strength was determined according to the ASTM C 393. Five specimens of 1220mm x 203mm x 120.6mm (48in. x 8in. x 4.75in) and support span 1092mm (43in.) were used for testing. A steel beam fixture was designed and built for the test then attached to the MTS-880 universal testing machine Fig. 3 shows pictures of test setups. Rubber pads with a shore hardness of 60 were placed between the specimen and the load contact points to avoid local failure. The load was applied at a uniform rate of 1.5mm/min. (0.06in./min). A linear variable differential transformer (LVDTs) was placed at the mid-span of the section to record the deflection of the samples. To measure the axial strains the electrical high precision strain gauges with three-wires that had a gauge length of 0.125 in and a resistance of 350 ohm were used.

The experimental results of bending tests on simply-supported CSIPs are presented in load versus deflection curve Fig. 4. The behavior of panels under the uniform static load was linear elastic up to the peak. After the peak, the loads start dropping due to the excessive deflection in the low density polyurethane foam Fig. 5. The maximum vertical force for the wall panel was 4448.2 N at the deflection 91.44 mm (3.6 in.) which corresponded to the maximum pressure the sample can handle was $181N/m^2$. One difference was the appearance of a discrete crack on the upper facesheet near the

load distributer fixture in the test panel number 2 due to the bending support moment (Fig. 6).

For all specimens, the test was stopped due to the excessive deflection reach 1/3 of the total thickness except for Sample 4 and 5, which were tested to failure in bending Fig. 7 at increasing load velocity with crosshead speed 12mm/min (0.5in/min) to examine the effect on residual deformations and stiffness degradation. The effect of loading velocity was clear in load- deflection curve Fig. 8, the elastic region is less than applying the load slowly and the failure start early. At the end of the test, it was noticed that the samples had a defect of a horizontal crack in the foam core, near to the top facesheet and debonding. The failure mechanisms were similar for samples 4,5 the lower facesheet first failed at normal strain of 0.050–0.055% and the maximum flexural strength 5.1MPa.

The stress-strain behavior of the facesheet in the longitudinal direction at mid-span, shown in Fig. 9, is quite linear. This is because the mid-span deflections which is affected by the shear deformations of the polyurethane core, which is typically a nonlinear material, while facesheet strains are only a reflection of the GFRP liner material. Also, the maximum strains measured on the compression and tension GFRP skins (Fig.9) were significantly lower than the flexural strain of the GFRP facesheet material of 4.96 %. In fact, failure occurred due to excessive deflection and shear deformation. This was a direct result of the excessive shear deformation of the low density polyurethane foam.

Since Young's modulus of the glass fiber reinforced polymer (GFRP) facesheet is significantly higher than that of the polyurethane foam. The theoretical flexural rigidity D (flexural stiffness EI) value was calculated with the sum of flexural rigidities shown in equation bellow which was 28.55 N-m$^2$.

$$D = EI = E_f \frac{bf^3}{6} + E_f \frac{fbd^2}{2} + E_c \frac{bc^3}{12} \tag{1}$$

Where $E_f$ is the facesheet modulus, $E_c$ is the core modulus, b is the width of the sandwich structure, d is the distance between the facesheet center, and f is the facesheet thickness, and c, is the core thickness.

The facesheet modulus was 19534 MPa obtained from previous studies [13]. The modulus of the PU foam is 4.48 MPa this value was obtained from the manufacturing data sheet. The CSIP's were compared to SIP's manufactured by Thermo core company (OBS wall panels) when a polyurethane core is used and with facesheet thickness 10.41mm (0.41 in.) based on the bending test. The CSIP's show better flexural properties as show in table 1.

### 4.2 Finite Element Analysis

A quasi-static three-dimensional finite element model has been developed to simulate the mechanical behavior of PU sandwich structure under four-point flexural loading. PU sandwich structure consists of three layers woven E-glass/polyurethane at the top and bottom, and low density polyurethane foam core in between. Face sheets and foam core were meshed using 8-node quadrilateral reduced-integration continuum shell element and 8-node linear reduced-integration hexahedral element, respectively. Hourglass control was applied to both element types to avoid zero-energy mode.

To reduce the computational cost, half of overall structure was modeled utilizing symmetry along the length direction, and both supports and steel loading heads were modeled as rigid body. Rigid four-node bilinear shells element was applied to mesh both supports and loading heads. Finite element mesh for the assembly is shown in Fig 10. Mechanical properties of woven E-glass/polyurethane and low density polyurethane foam core are listed in Table 2. The support was constrained except the rotation along Z direction. For loading head, all degrees of freedom, except for the displacement along Y direction and rotation along Z direction, were constrained. The symmetric boundary condition was applied on the symmetric surface. Hard contact property in the normal direction was applied in the interaction between loading head/top face sheet, and support/bottom face sheet. Displacement loading was applied on the loading head.

In this study, nonlinear finite element analysis was conducted considering the combined effects of the linear elastic behavior of laminates and the nonlinear behavior of foam core, and only the initial part of mechanical response before ultimate failure under flexural loading was investigated. Comparison between simulation results and experimental data in term of loading force versus extension before ultimate rupture is illustrated in Fig. 11. A good correlation between simulation results and experimental data can be observed.

Figure 12 shows S11 contour in low density foam core. It can be observed that the maximum compressive stress is 29.9 kPa, which is located at the top foam surface near the loading head. Fig.13 shows the S11 contours of the topmost layer in the top face sheets, and bottommost layer in the bottom face sheets, respectively. The compressive S11 stress in the top face sheets near the loading heard and the tensile S11 stress in the bottom face sheets near the support can be clearly observed. The absolute S11 values in both locations are much larger than S11 values in the foam core, indicating that the face sheets absorbed most of in-plane loading and bending moment.

## 5- THERMAL PERFORMANCE SIMULATION

The effectiveness of using PU-CSIP panel, consists of a single core of 2 lb/ft$^3$ (32kg/m$^3$) density polyurethane foam and laminated on both sides by polyurethane composite facesheets, was studied in this part under two categories transient thermal behavior and energy saving calculations. In each part, the PU-CSIP results were compared to the results of expanded polystyrene (EPS) and extruded polystyrene (XPS) cores with oriented strand board (OSB) facesheets. The latest two SIPs are denoted in this work as EPS-SIP and XPS-SIP, respectively. The comparison was conducted using the same panel geometry as based on the cross-section shown in Fig. 14.

### 5.1 Transient Thermal Behavior

One dimensional transient heat conduction simulation was conducted using ABAQUS (version 6.11) for a 3-D geometry. The geometry was a composite panel with dimensions 6m x 3m x 0.1143m (236.22in x 118.11in x 4.5in) of height, width and

thickness, respectively. An 8-node linear standard heat transfer brick element (DC3D8) of total 1800 elements was used in this simulation. Properties of the materials like thermal conductivity (K), specific heat capacity ($C_p$) and density ($\rho$) are, if not specified, obtained from literature [14] and listed in Table 3. The thermal properties of the composites polyurethane facesheet determined experimentally using thermal properties analyzer (QuickLine-30).

The required properties of core, facesheet are assigned to the geometry to run the simulation. External uniform temperature boundary condition and initial temperature condition were set to 40°C and 20°C, respectively, to simulate panel temperature distribution for 1 hr and 12 hr. Initial temperature condition was set as a predefined field for the whole geometry in the initial step. As insulated boundary condition is not defined in ABAQUS, all other edges were insulated by applying a uniform surface heat flux of $1\times10^{-17}$ W/m$^2$ (Fig. 15). Temperature distribution for PU-CSIP simulation after 12 hr is shown in Fig. 16. Temperature distribution through the thickness results for the three types of panel is shown in Fig. 17.

Simulation results indicate that after 12 hr the temperature distribution on the other side of the panel is almost equal 40°C, especially for EPS-SIP, which is the boundary condition of the external surface. Accordingly, as the internal surface temperature approaching the external temperature, the case is almost a steady state. Temperature distribution for transient heat conduction is dependent on the thermal diffusivity (D) of the material.

$$D = \frac{k}{\rho \times Cp} \tag{2}$$

where $k$, $\rho$ and $Cp$ are defined in Table 3. Materials with low thermal diffusivity have lower temperature at any spatial point after a certain time [15]. For a composite slab the following equation is used to determine the effective thermal conductivity ($k_{eff}$)

$$k_{eff} = \frac{L_1 + L_2 + L_3}{L_1/k_1 + L_1/k_1 + L_1/k_1} \tag{3}$$

Where $L$ is the layer thickness of the composite slab materials. Calculated effective thermal conductivities of the three panels were found 0.0283 W/m·k, 0.0301 W/m·k and 0.0380 W/m·k for PU-CSIP, XPS-SIP and EPS-SIP, respectively. Using rule of combined wall effective thermal diffusivity ($D_{eff}$) of the composite slab [12].

$$D_{eff} = \frac{v_1 k_1 + v_2 k_2 + v_3 k_3}{v_1 \, k_1 / D_1 + v_2 \, k_2 / D_2 + v_3 \, k_3 / D_3} \tag{4}$$

Where $v$ is the volume fraction of the layer in the composite slab. In the present case, as the whole layers have the same area ($A$), equation (4) can be written.

$$D_{eff} = \frac{L_1 k_1 + L_2 k_2 + L_3 k_3}{L_1 \, k_1 / D_1 + L_2 \, k_2 / D_2 + L_3 \, k_3 / D_3} \tag{5}$$

Calculated effective thermal diffusivities of the three panels were found $2.92 \times 10^{-7}$ 1/s, $3.48 \times 10^{-7}$ 1/s and $5.17 \times 10^{-7}$ 1/s for PU-CSIP, XPS-SIP and EPS-SIP, respectively. In Fig.17, XPS-SIP shows better transient response than EPS-SIP. However, PU-CSIP shows the best response as compared to the others, or PU composite panels have lower overall thermal diffusivity as shown in calculations above. However, XPS-SIP may show better transient response for higher densities XPS-core like 48 kg/m$^3$, but thermal conductivity of PU-core foam is still lower which means better $R$ value, known as thermal resistance. In general, transient behavior shows the effect of the thermal diffusivity but not only the conductivity factor. The effect of thermal conductivity is better shown when studying energy consumption in the next section. Also, energy is the final target when using CSIP in housing which gives a significant sense of the reason behind this use.

## 5.2 Energy Consumption Calculation

A small house of the dimensions 8m x 6m x 4.5m (314.961in. x 236.22in. x 177.165in.) and orientation shown in Fig.18 was proposed for the sake of site energy consumption calculations. The house is located in Rolla, MO for which Table 4 shows the general house location. Residential buildings characteristics as required by IECC 2009 code [16, 17] were taken into account to have realistic results of energy consumption. The present house was considered as a single zone building intended for one family of occupancy 4 persons. It means that the house interior is a single zone with no details in which ASHRAE 55-2004 comfort index of air flow requirements, as an example, may not be satisfied. However, this is warranted as the main goal is to check energy consumption rather than house design. The present house has two windows (one facing the north and the other one facing the south) with a total area ratio of 3.57%, which complies with the IECC 2009 code of 15% maximum. Also, floor to ceiling height code value is required to be 3.048m (10 ft) in where it was proposed as 3 m in the present case. All other elements like internal loads, HVAC (Heating, Ventilation and Air-Conditioning) and exterior lighting were made to meet the above code requirements (Table 5).

EnergyPlus™ (version 8.0.0.008) was used to calculate the energy consumption during 365 days. The required weather file for the present envelope was obtained from the U.S. Department of Energy. Heating and cooling thermostat setpoint schedules were based on a constant indoor temperature of 20˚C (68˚F) and 25.6˚C (78˚F). The calculation was conducted for the three different wall materials. Assume that the whole three houses were built with CSIP's, EPS-SIP's and XPS-SIP's with the exception of the floor. ASRAEE 2005 material properties data base, included in EnergyPlus™, was used to obtain the light floor, door wood and widow glass properties and thickness (Table 6).

Indoor and outdoor daily temperature distribution is shown in Fig.19. Results of annual energy consumption for the three types of panels are listed in Table 7. Based on these results, energy consumption is almost the same for the three materials. These results

are warranted and could be interpreted based on the relative difference in thermal properties of the panel materials of the present work.

All energy code requirements are based on the *R* value, mainly dependent on *k*, as shown below for a conductive resistance

$$R = \frac{L}{kA}$$

(6)

However, there is a slight difference in effective thermal conductivity of the panels materials as calculated above. This is the reason behind almost same annual energy consumption as steady state thermal conduction is dependent on the thermal conductivity value *(k)* or the conductive resistance *(R)*. Since energy balance of the annual simulation, in most of the year, is steady state based simulation, the effect of k is dominating over the heat transfer calculations.

In order to verify these energy consumption results, a comparison with energy end uses per unit area of two locations were conducted. A ranch house model was proposed to be located in Chicago, IL and Orlando, Florida [14]. As a comparison, the thermostat setpoint of the present work and ranch house model is the same. Based on the results of annual simulation for these locations, it was found that end uses energies per unit area were 0.69 $GJ/m^2$ and 0.4986 $GJ/m^2$ for Chicago, IL and Orlando, Florida, respectively. For the present work, the end uses energy per unit area was 0.674 $GJ/m^2$ for the current location. For Orlando, Florida location the space heating consumption was 0.7% of the total annual energy while the consumption of Chicago, IL was 35.8%. In the present location, it was 29.3%, 30.3% and 33.6% for PU- CSIP, XPS-SIP and EPS-SIP, respectively. The envelope of this case shows intermediate energy consumption in between thereof two locations.

## 6- CONCLUSION

Composite structural insulation panels were manufactured using thermoset polyurethane resin systems. The PU CSIP's manufactured successfully using modify

VARTM process and have been investigated in flexure test mechanical and numerically. In addition the thermal properties have been simulated and compared to EPS and XPS with oriented strand board (OSB) using finite element analysis. Energy consumption calculation conducted to whole hose made of PU composite materials and compared to EPS and XPS with OSB materials used EnergyPlus software based on Missouri State code. Based on experimental and numerical analysis of the innovative composite sandwich structure insulation panels CSIP with polyurethane foam polyurethane facesheet the following conclusions can be drawn from the research:

1- The PU CSIP's not only increase the strength but enhance ductility too. In addition, sandwich panels made by bidirectional FRP provide ductility and toughness more than those made using the OSB factsheet

2- VARTM method is the best processing method for manufacturing the CSIP's with soft foam due to its high efficiency in achieving adequate bond between FRP laminates and PU foam

3- CSIPs are characterized by a higher strength to weight ratio. They are also resistant to biological degradation in contrast to traditional SIPs

4- Under uniformly distributed loads, panels with 'soft' core underwent very large deflections associated with excessive shear deformation of the core, leading to a highly nonlinear behavior. However, no physical failure was observed

5- No significant stiffness degradation has taken place. However, it is clear that some permanent deflection has occurred upon unloading. This permanent deflection is clearly larger in specimen 4, 5. It is noted that the specimen with a soft core has a higher capacity of energy dissipation

6- Based on the thermal simulation results the CSIP's with PU foam showed better thermal insulation than EPS and XPS foam with OSB facesheet

7- A three-dimensional finite element model was developed using commercial software ABAQUS for PU CSIP's under four-point flexural loading and validated by the experimental results. The results show a good correlation between simulation results and experimental data.

# 7-  REFERENCES

[1] Caijun S, Fouad H.F. "Autoclaved Aerated Concrete-properties and structural design," American Concrete Institute, Special Publication ISBN-13: 978-0870311758226, 2005.

[2] M. A. Mousa and N. Uddin, "Experimental and analytical study of carbon fiber-reinforced polymer (FRP)/autoclaved aerated concrete (AAC) sandwich panels," Engineering Structures, Vol. 31, pp. 2337-2344, 2009.

[3] L. Cheng and V. M. Karbhari, "New Bridge Systems using FRP Composite and Concrete: A State of-the-art Review," Journal of Structural Engineering Materials, Vol. 8, pp. 143-154, 2006.

[4] L. Smakosz, J. Tejchman, "Evaluation of strength, deformability and failure mode of composite structural insulated panels," Journal of Materials and Design, Vol. 54, pp. 1068–1082, 2014.

[5] T. Sharaf, W. Shawkat and A. Fam, "Structural Performance of Sandwich Wall Panels with Different Foam Core Densities in One-way Bending," Journal of Composite Materials, Vol. 44, No. 19, pp. 2249-2263, 2010.

[6] R. R. Vuppalapati, k. Chandrashekhara, T. P. Schuman, "Manufacturing and performance evaluation of core-filled pultruded bio-composite panels," Proceedings of the annual ISC research symposium , Rolla, MO; (April 14, 2009)

[7] A. Bezazi, A. El Mahi, J.M. Berthelot, "Experimental Analysis of Behavior and Damage of Sandwich Composite Materials in Three-point bending. part 1. Static Tests and Stiffness degradation at failure studies," Journal of Strength of Materials, Vol. 39, No. 2, pp.170-177, 2007.

[8] J. D. Kelso, PE, "Buildings Energy Data Book," Prepared for the Buildings Technologies Program Energy Efficiency and Renewable Energy U.S. Department of Energy, (March 2012).

[9] T. Kawasaki and S. Kawai, "Thermal insulation properties of wood-based sandwich panel for use as structural insulated walls and floors," Journal of Wood Science, Vol. 52 (1), pp. 75-83, 2006.

[10] S.R. Hastings, "Breaking the-heating barrier – Learning from the first houses without conventional heating," Energy and Buildings, Vol. 36, pp. 373-380, 2004.

[11] J. E. Christian,  L. Richards, P. Childs, J. Atchley and H. Moon "Energy Efficiency, SIPS, Geothermal, and Solar PV Used in Near Zero-Energy House," American Society of Heating, Refrigerating and Air-Conditioning Engineers, Published in ASHRAE Transactions, Vol. 112, Part 2, 2006.

[12] N. Hester, K. Li, J. R. Schramski and J. Crittenden, "Dynamic modeling of potentially conflicting energy reduction strategies for residential structures in semi-arid climates," Journal of Environmental Management, Vol.  97, pp. 148-153, 2012.

[13] M. Mohamed, Z. Huo, S. Hawkins, V. Birman, J. Volz and K. Chandrashekhara "Moisture Effects on Performance of Polyurethane Composite Sandwich Panels Manufactured using VARTM," Proceedings of SAMPE Conference, Long Beach CA, pp. 1-15, May 6-9, 2013.

[14] M. K. Kumaran, "Hygrothermal Properties of Building Materials," MANUAL ON MOISTURE ANALYSIS IN BUILDINGS, Copyright by ASTM Int'l (all rights reserved); Mon Oct 14 00:15:08 EDT , 2013.

[15] D. Thomas, S. C. Mantell, J. H. Davidson,  L. F. Goldberg and J. Carmody "Analysis of Sandwich Panels for an Energy Efficient and Self-Supporting Residential Roof," Journal of Solar Energy Engineering, Vol. 128, pp. 338-348, 2006.

[16] A. Salazar, "On thermal diffusivity," EUROPEAN JOURNAL OF PHYSICS, Vol. 24, pp.  351–358, 2003.

[17] Y. Huang and K. Gowri, "Comparison of 2006 IECC and 2009 IECC Commercial Energy Code Requirements for Kansas City, MO," Available to the public from the National Technical Information Service, U.S. Department of Commerece, Springfield, VA, March 2011

Table 1 Comparison test results of CSIP's and SIP's

| Property | CSIP's | SIP's (OBS Termocore panels) |
|---|---|---|
| Maximum Load (N) | 4448.2 | 3576 |
| Deflection at Max Load mm (in) | 91.44 (3.6) | 21.8 (0.86) |
| Flexural Strength (MPa) | 5 | -- |
| Maximum Stress (MPa) | 11.2 | 2.9 |
| Flexural Stiffness (kN-m$^2$) | 28.55 | 18.6 |

Table 2 Mechanical properties of woven E-glass/Polyurethane and low density foams

| Material | Property | Value |
|---|---|---|
| Woven E-glass/Polyurethane | Longitudinal Modulus, $E_x$ (GPa) | 19.5 |
| | Transverse Modulus, $E_y$ (GPa) | 19.5 |
| | Poisson's ratio, $v$ | 0.13[*] |
| | In-plane Shear Modulus, $G_{12}$ (GPa) | 5.5[*] |
| | Out-plane Shear Modulus, $G_{13}$ (GPa) | 5.1[*] |
| | Out-plane Shear Modulus, $G_{23}$ (GPa) | 5.1[*] |
| Low Density Polyurethane Foam | Compressive Modulus, E (MPa) | 2.83 |
| | Poisson's ratio, $v$ | 0.3 |
| | Compressive Strength, $\sigma_t$ (KPa) | 117 |

Properties with '*' are approximated or obtained from literatures, others are from experiments

Table 3 Properties of materials used in simulation

| Material | $k$ (W/m·k) | $Cp$ ( J/kg·k) | $\rho$(kg/m$^3$) | $D^*$ (1/s)*10$^{-6}$ |
|---|---|---|---|---|
| EPS | 0.037 | 1470 | 14 | 1.79786 |
| XPS | 0.029 | 1470 | 26 | 0.75876 |
| OSB facesheet | 0.12 | 1880 | 640 | 0.099734 |
| PU facesheet | 0.3518[**] | 837[**] | 1876[*] | 0.224046 |
| PU foam[***] | 0.027 | 2291 | 32 | 0.368206 |

\* Determined experimentally by water displacement according to ASTM D792, \*\* Determined experimentally, \*\*\* Manufacturers data sheet

Table 4 Envelope location parameters

| Parameter | Value |
|---|---|
| Latitude (deg) | 38.13 |
| Longitude (deg) | -91.8 |
| Elevation (m) | 336.00 |
| Time Zone | -6.0 |
| North Axis Angle (deg) | 0.00 |
| Rotation for Appendix G (deg) | 0.00 |
| Hours Simulated (hrs) | 8760.00 |

Table 5 Interior and exterior loads of sample house

| Load type | Value |
|---|---|
| Lighting power density | 3.875 W/m$^2$ |
| Plug load power density | 6.674 W/m$^2$ |
| Occupancy | 4 persons |
| Water heater | 10˚C, 49˚C (cold water and hot water temperature) |
| | 3.51×10$^{-6}$ m$^3$/s (80 gallon/day) (water demand) |

Table 6 Constructional materials of floor, door and window

| Construction type | Layers (outside to inside) |
|---|---|
| Light floor | F16 acoustic tile, F05 air and M11 100 mm light weight concrete |
| Door | G07 100 mm wood |
| Window | 3 mm clear glass |

Table 7 Annual energy consumption of sample house

| Panel type | PU- CSIP | XPS-SIP | EPS-SIP |
|---|---|---|---|
| Total Site Energy (GJ) | 32.38 | 32.78 | 34.89 |

Figure 1 The cross section of the polyurethane composite insulation structural
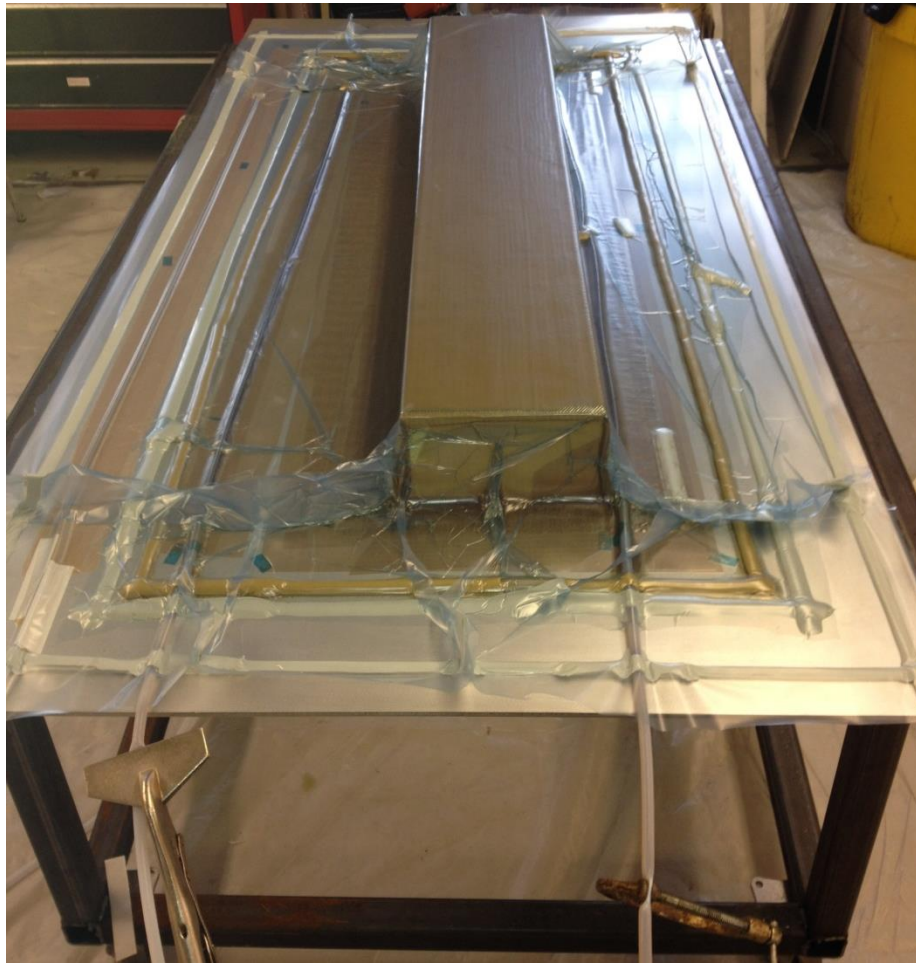
Figure 2 Shows VARTM process set up
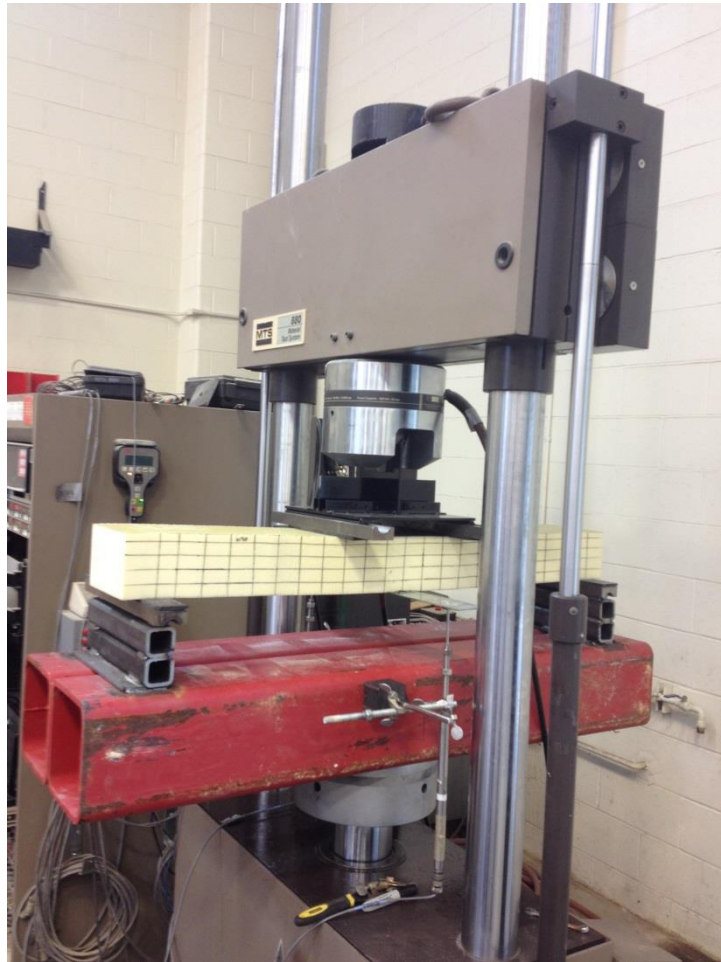
Figure 3 Shows picture of four bending test setup
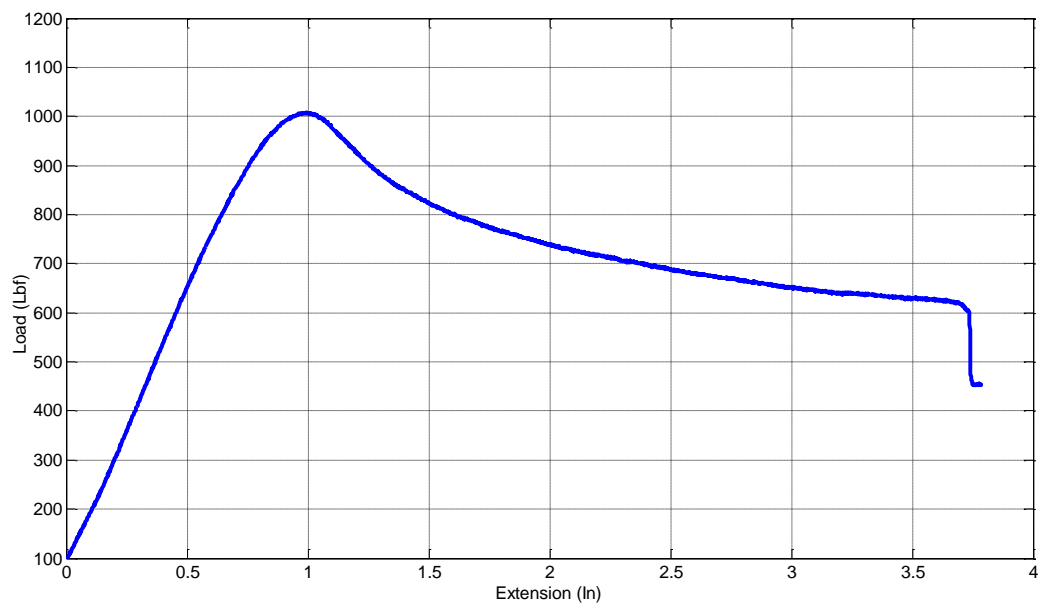
Figure 4 Shows load vs. deflection at the mid-span



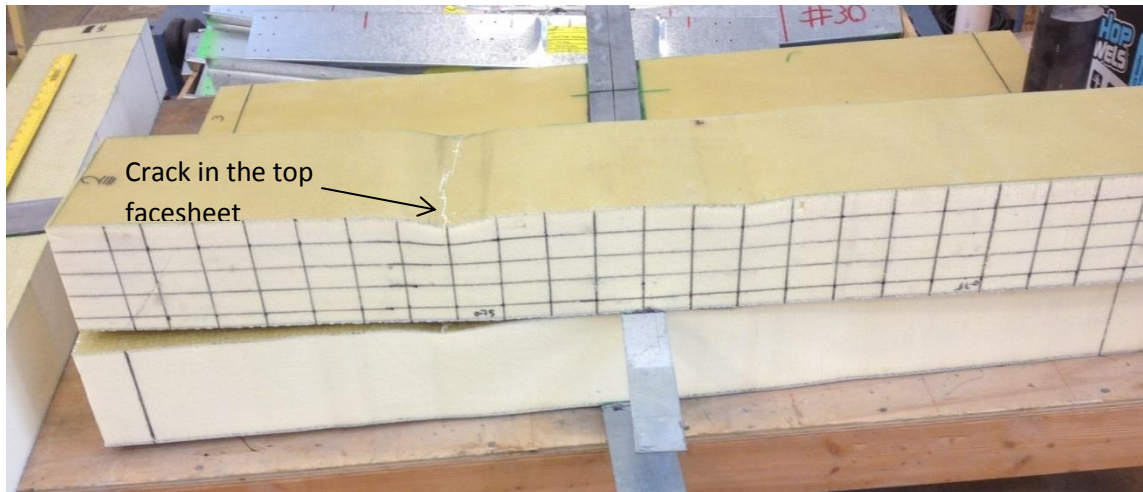Figure 5 Shows panel deflection during the test

Figure 6 Shows discrete crack on the top facesheet



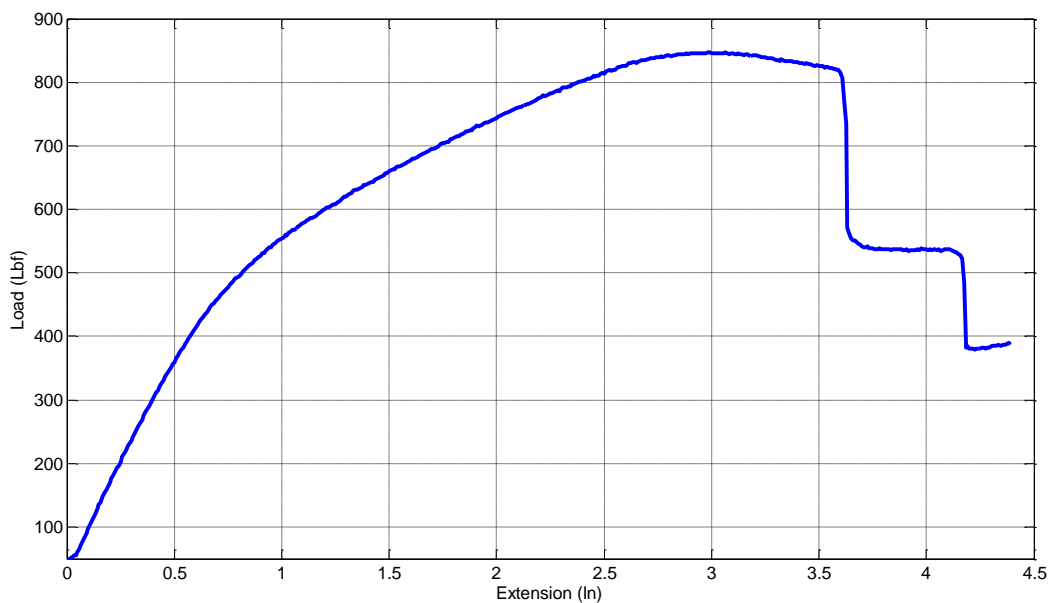Figure 7 Shows applying bending load up to failure occurred

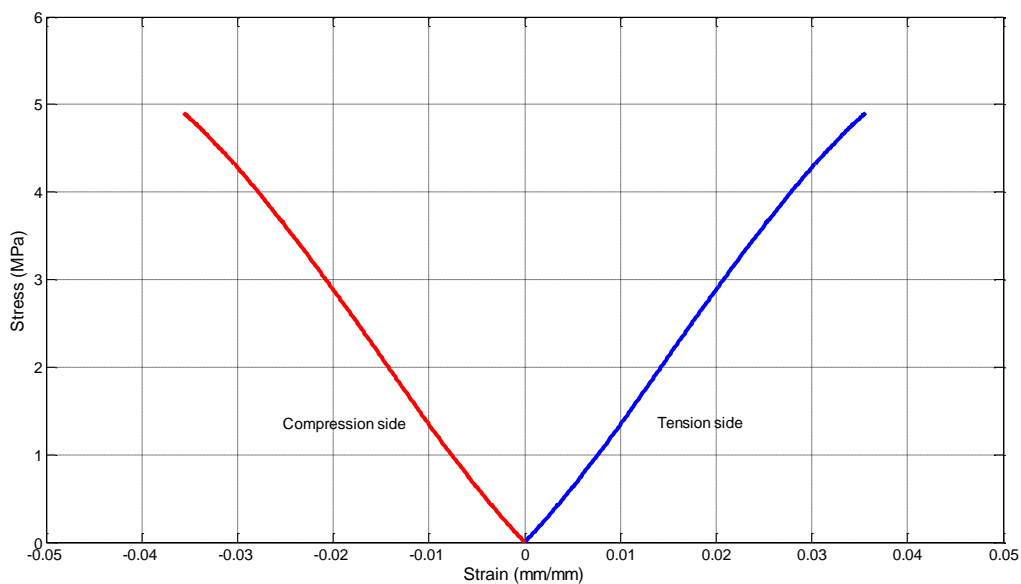Figure 8 Shows load vs. deflection for samples tested up to failure with
crosshead speed 0.5in./min



Figure 9 Stress-strain behavior of the facesheet in the longitudinal
direction at mid-span
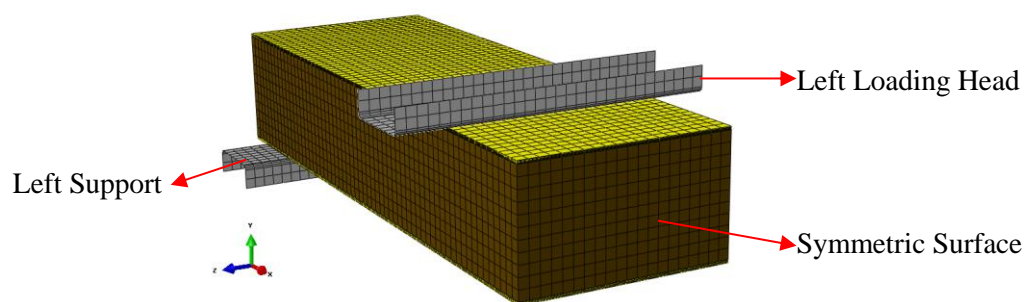
Figure 10 Finite element mesh for the assembly
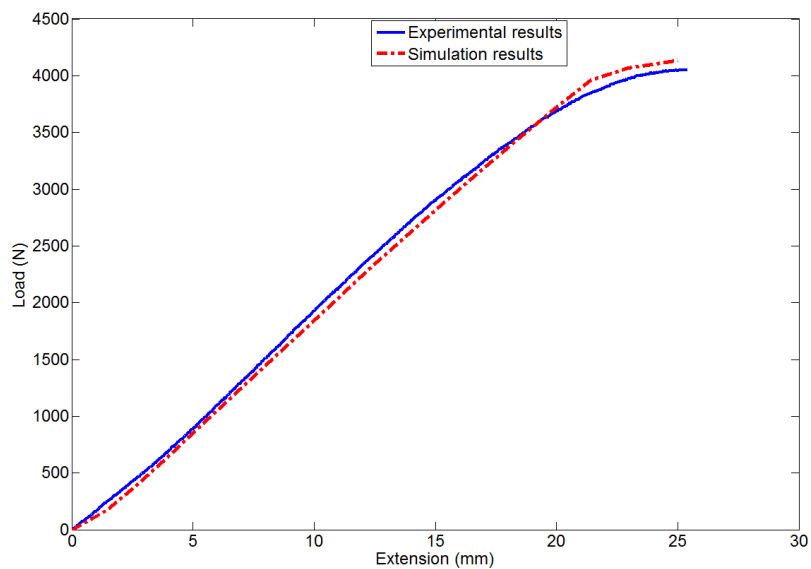


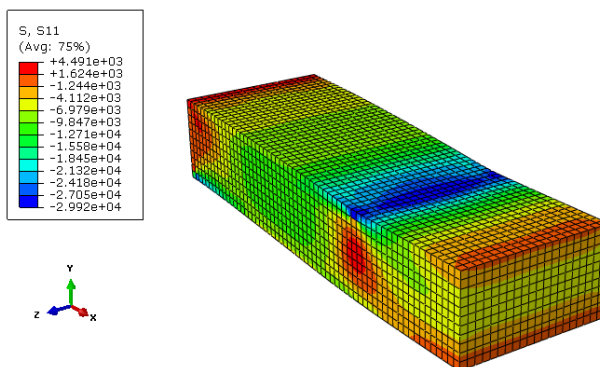Figure 11 Comparison of loading force vs. extension between simulation and experimental results

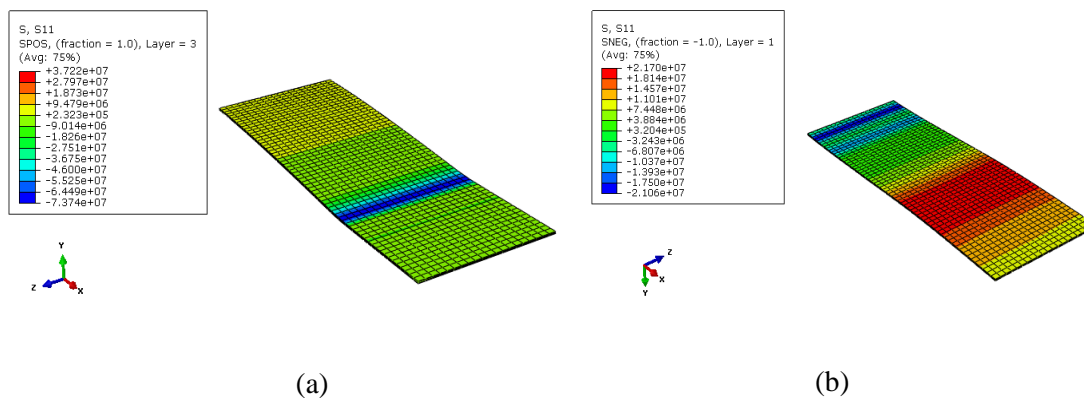Figure 12 Stress (S11) contour in the foam core



(a)

(b)

Figure 13 Stress (S11) contours on (a) topmost layer in the top face sheets, and (b) bottommost layer in the bottom face sheets
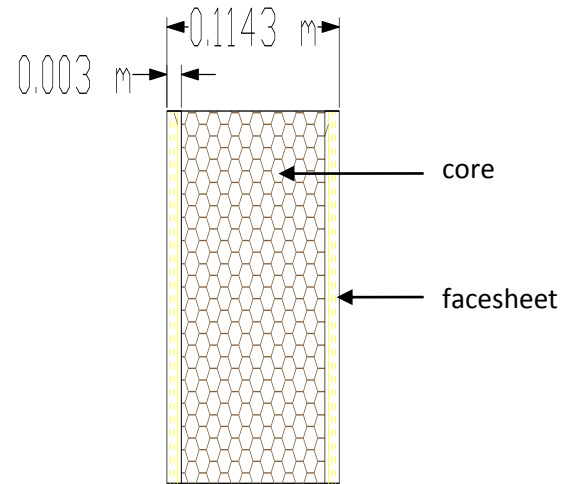
Figure 14 Panel cross-section of the present work (not to scale)
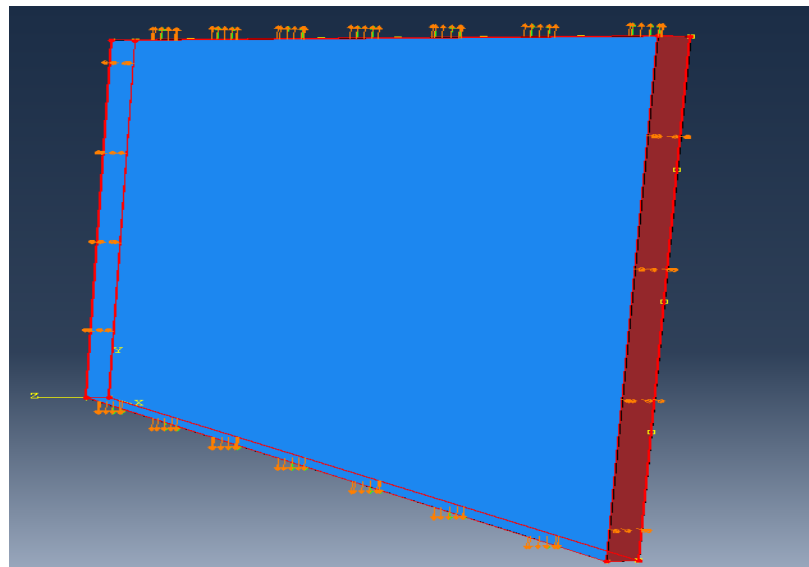


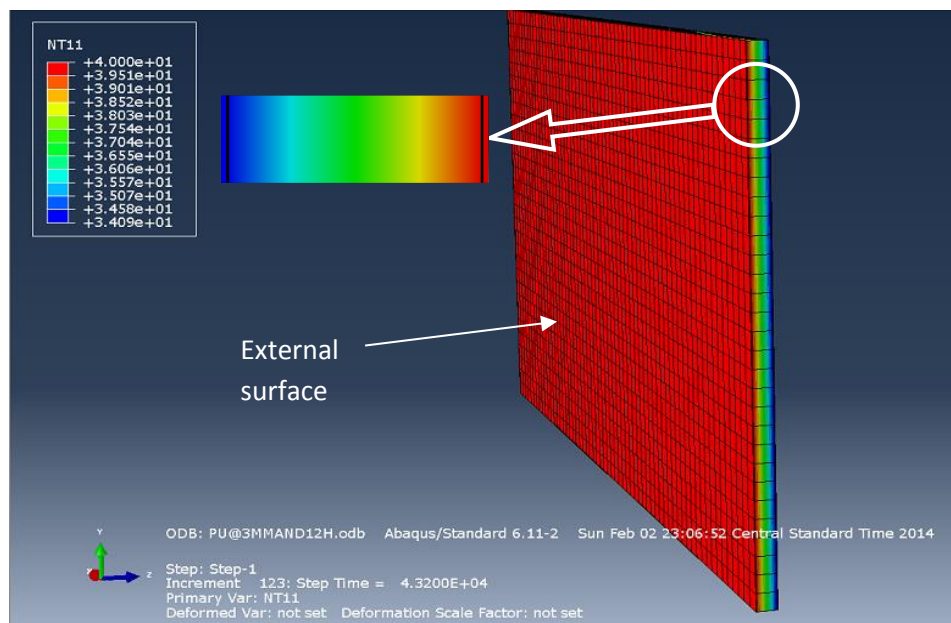Figure 15 Applying the boundary condition to edges

Figure 16 Temperature distribution, PU-CSIP after 12 hr
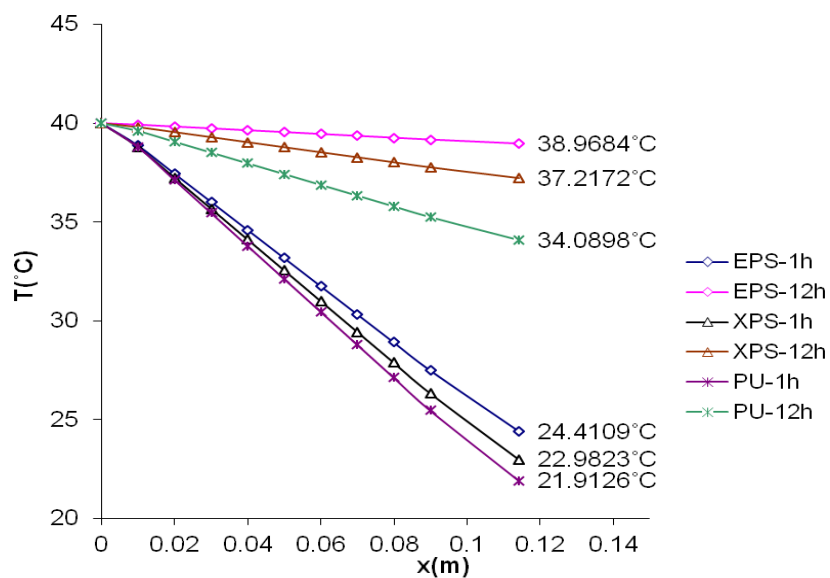


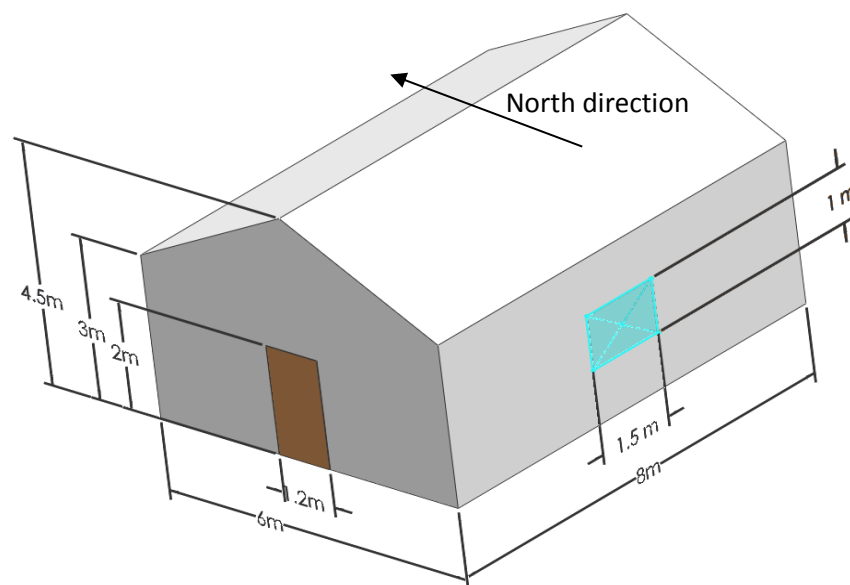Figure 17 Through thickness temperature distribution

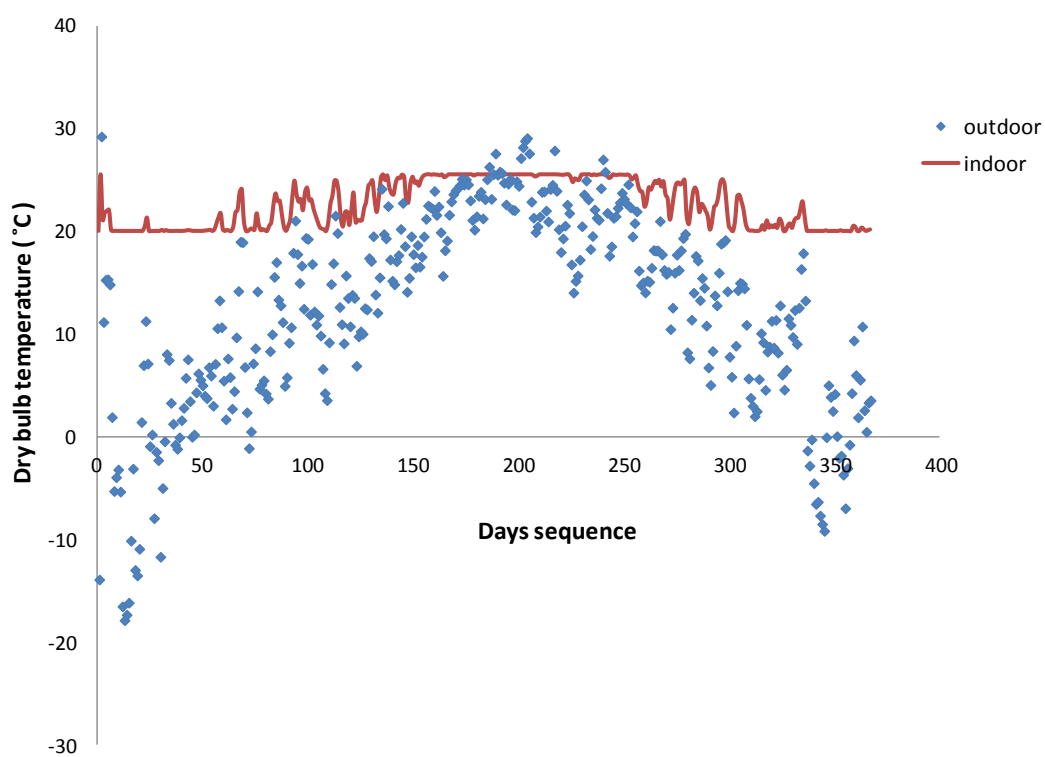Figure 18 House dimensions and orientation



Figure 19 Daily indoor and outdoor temperature distribution

**SECTION**

**3- CONCLUSION**

The dissertation presents the performance evaluation and characterization of polyurethane composites materials using vacuum infusion process. In paper I carry out comparison and evaluation of mechanical performance of two different polyurethane resin systems. In order to make decision of what PU will be used in task II and task III. Glass fiber composites were designed using these two different resin systems and were fabricated using cost effective process VARTM process. Fundamental properties include strength and modulus were measured and analyzed for the behavior of two resin systems. Thermal mechanisms were studied using differential scanning calorimeter (DSC) and the viscosity profile was analyzed using Brookfield LVD-II programmable rotational type viscometer. Based on the results the two-part PU resin system was chosen for farther.

In the second paper, three designs of glass reinforced composite sandwich structures, namely boxes (web-core W1), trapezoid and polyurethane rigid foam, are fabricated using new generation of two-part thermoset polyurethane resin systems as matrix materials with vacuum assisted resin transfer molding (VARTM) process. The stiffness, load-carrying capacity and compressive strength were evaluated. Core shear, flatwise and edgewise compression tests were carried out for these three models. The mechanical response of three designs of sandwich structures under flexural loading were analyzed using commercial finite element method (FEM) software ABAQUS. It is suggested that sandwich panels with prisma cores represent a feasible design for full scale bridge decks. The simulation results of flexural behavior were validated by experimental findings.

In the third paper, successfully usage of glass fiber reinforced two-part PU composite to design and manufacture composite structure insulation panels CSIP. The study conducted a comparison two systems for wall panels, the first one by using oriented strand board (OSB) and core material (BASF Autofroth 2-part Foam: 9300A Isocyanate)

manufactured by Thermocore of Missouri, LLC and the second CSIP by using thermoset polyurethane resin systems as matrix, bidirectional E-glass fiber as reinforcement materials and 2.00 lb density polyurethane foam core manufactured with VARTM at Missouri S&T composite lab. To assess a small-scale E-glass/PU panel's performance under a four-point bending test, energy efficient and discuss results in terms of load, deflection and energy was saving. Based on the results the PU CSIP's increase the strength and enhance ductility too. In addition, sandwich panels made by bidirectional FRP provide ductility and toughness more than those made using the OSB factsheet. The results from the present work show that polyurethane composite can be used in vacuum infusion processes and are very promising in producing parts that have part qualities comparable to other resin systems.

**BIBLIOGRAPHY**

1. B. D. Agarwal, L. J. Broutman, and K. Chandrashekhara, "Analysis and Performance of Fiber Composites," Third Edition, John Wiley & Sons, Inc., New Jersey, 2006.

2. M. Yeats, and D. Slaback, "Process and product improvements with the use of polyurethanes in pultrusion," Technical Paper - Society of Manufacturing Engineers. EM, pp. 1-7, 2002.

3. C. Hopmann, E. Michaeli, and T. Preuss, "Pultrusion - Polyurethane (PU) as Alternative for Conventional Matrix Systems," International SAMPE Technical Conference, pp.1-11, May 23-27, Long Beach, CA, 2011.

4. J. Haynes and C. Snyder, "Structural, Environmental and Processing Advantages of Polyurethane Pultrusion," JEC Composites Magazine, Vol. 45, pp. 38, 2008.

5. M. Connolly, J. King, T. Shidaker, and A. Duncan, "Processing and Characterization of Pultruded Polyurethane Composites," Proceedings of the 8$^{th}$ World Pultrusion Conference (European Pultruders Technical Association), pp. 1-16, March 23-24, Budapest, Hungary, 2006.

6. R. Karakuzu, E. Erbil, and M. Aktas, "Impact Characterization of Glass/Epoxy Composite Plates: An Experimental and Numerical Study," Composite Part-B, Vol. 41, pp. 388-395, 2010.

7. U. Younes, "Development of PU-based RTM and VARTM Technology," Composites 2010, pp. 1-17, February 9-11, Las Vegas, NV, 2010.

8. J. Tate, A. Akinola, P. Patel, and J. Massingill, "Nano-modified Soy-based Polyurethane/E-glass Composites-Mechanical and Thermal Properties," International SAMPE Symposium and Exhibition, pp. 1-10, May 18-21, Baltimore, MD, 2009.

9. J. Tate, J. Massingill, P. Patel, and S. Konga, "Enhancement in Mechanical Properties by Improving Fiber/Matrix Adhesion in Bio-based Polyurethane/E-glass Composites," International SAMPE Symposium and Exhibition, pp. 1-10, May 18-22, Long Beach, CA, 2008.

10. J. Tate, J. Massingill, P. Patel, P. Rikka, and S. Arabie, "Mechanical Characterization of Bio-based Polyurethane/E-glass Composites," International SAMPE Fall Technical Conference , pp. 1-10, October 29- November 1, Cincinnati, OH, 2007.

11. Y. Zhang, P. Zhu, and X. Lai, "Finite Element Analysis of Low-Velocity Impact Damage in Composite Laminated Plates," Materials and Design, Vol. 27, pp. 513-519, 2006.

12. Z. Aslan, R. Karakuzu, and B. Okutan, "The Response of Laminated Composite Plates under Low-Velocity Impact Loading," Composite Structures, Vol. 59, pp. 119-27, 2003.

13. R. Tiberkak, M. Bachene, S. Rechak, and B. Necib, "Damage Prediction in Composite Plates Subjected to Low Velocity Impact," Composite Structures, Vol. 83, pp. 73-82, 2008.

14. Y. Shi, T. Swait, and C. Soutis, "Modelling Damage Evolution in Composite Laminates Subjected to Low Velocity Impact," Composite Structures, Vol. 94, pp. 2902-2913, 2012.

15. J. Fan, Z. Guan, and W. Cantwell, "Modeling Perforation in Glass Fiber Reinforced Composites Subjected to Low Velocity Impact Loading," Polymer Composites, Vol. 32, pp. 1380-1388, 2011.

# VITA

Mohaned Mohamed was born in Tobruk, Libya. He was admitted to Omer Al-Mokhtar University, Libya in 1996 and received his Bachelor's degree in Mechanical Engineering in 2001. He continued his graduate study at Tabbin Institute for Metallurgical Studies, Cairo, Egypt, and received his M.S. degree in Mechanical Engineering in 2005. He worked at Omer Al-Mokhtar University, Libya as a lecturer in mechanical engineering department from October 2005 to March 2008.

Since January 2009, Mohaned Mohamed has been enrolled in the Ph.D. Program in Mechanical Engineering at Missouri University of Science and Technology, Rolla. He has served as Graduate Research Assistant between May 2013 and December 2014 in the Department of Mechanical and Aerospace Engineering. In December 2014, he received his Ph.D. degree in Mechanical Engineering from Missouri University of Science and Technology, Rolla, Missouri.